



JAEA-Data/Code
2023-012

DOI:10.11484/jaea-data-code-2023-012

JAEA-
Data/Code

Data Report of ROSA/LSTF Experiment TR-LF-15

—Accident Management Actions during Station Blackout Transient
with Pump Seal LOCA—

Takeshi TAKEDA

Reactor Safety Research Division
Nuclear Safety Research Center
Sector of Nuclear Safety Research and Emergency Preparedness

October 2023

Japan Atomic Energy Agency

日本原子力研究開発機構

本レポートは国立研究開発法人日本原子力研究開発機構が不定期に発行する成果報告書です。
本レポートはクリエイティブ・コモンズ表示 4.0 国際ライセンスの下に提供されています。
本レポートの成果（データを含む）に著作権が発生しない場合でも、同ライセンスと同様の
条件で利用してください。（<https://creativecommons.org/licenses/by/4.0/deed.ja>）
なお、本レポートの全文は日本原子力研究開発機構ウェブサイト（<https://www.jaea.go.jp>）
より発信されています。本レポートに関しては下記までお問合せください。

国立研究開発法人日本原子力研究開発機構 JAEA イノベーションハブ 研究成果利活用課
〒 319-1195 茨城県那珂郡東海村大字白方 2 番地 4
電話 029-282-6387, Fax 029-282-5920, E-mail:ird-support@jaea.go.jp

This report is issued irregularly by Japan Atomic Energy Agency.
This work is licensed under a Creative Commons Attribution 4.0 International License
(<https://creativecommons.org/licenses/by/4.0/deed.en>).
Even if the results of this report (including data) are not copyrighted, they must be used under the
same terms and conditions as CC-BY.
For inquiries regarding this report, please contact Institutional Repository and Utilization Section,
JAEA Innovation Hub, Japan Atomic Energy Agency.
2-4 Shirakata, Tokai-mura, Naka-gun, Ibaraki-ken 319-1195 Japan
Tel +81-29-282-6387, Fax +81-29-282-5920, E-mail:ird-support@jaea.go.jp

Data Report of ROSA/LSTF Experiment TR-LF-15
—Accident Management Actions during Station Blackout Transient with Pump Seal LOCA—

Takeshi TAKEDA

Reactor Safety Research Division
Nuclear Safety Research Center
Sector of Nuclear Safety Research and Emergency Preparedness
Japan Atomic Energy Agency
Tokai-mura, Naka-gun, Ibaraki-ken

(Received August 23, 2023)

An experiment denoted as TR-LF-15 was conducted on June 11, 2014 using the Large Scale Test Facility (LSTF) in the Rig of Safety Assessment-V (ROSA-V) Program. The ROSA/LSTF experiment TR-LF-15 simulated accident management (AM) actions during a station blackout transient with TMLB' scenario with pump seal loss-of-coolant accident (LOCA) in a pressurized water reactor (PWR). This scenario is featured by loss of auxiliary feedwater functions. The pump seal LOCA was simulated by a 0.1% cold leg break. The test assumptions included total failure of both high pressure injection system and low pressure injection system of emergency core cooling system (ECCS). Also, it was presumed non-condensable gas (nitrogen gas) inflow to the primary system from accumulator (ACC) tanks of ECCS.

When steam generator (SG) secondary-side collapsed liquid level dropped to a certain low liquid level, the primary pressure turned to rise. After the SG secondary-side became voided, the safety valve of a pressurizer cyclically opened which led to loss of primary coolant. Core uncover thus took place owing to core boil-off at high pressure. When an increase of 10 K was confirmed in cladding surface temperature of simulated fuel rods, SG secondary-side depressurization was started as the first AM action. At that time, the safety valves in both SGs were fully opened. Primary depressurization was initiated by completely opening the pressurizer safety valve as the second AM action with some delay after the first AM action onset. When the SG secondary-side pressure lowered to 1.0 MPa following the first AM action, water was injected into the secondary-side of both SGs via feedwater lines with low-head pumps as the third AM action. A reduction in the primary pressure was accelerated because the heat removal from the SG secondary-side system resumed shortly after the third AM action initiation. The whole core was quenched by the recovery in the core liquid level due to coolant injection from the ACC system into both cold legs. The primary depressurization rate reduced on account of accumulation of nitrogen gas in the SG U-tubes.

This report summarizes the test procedures, conditions, and major observations in the ROSA/LSTF experiment TR-LF-15.

Keywords: PWR, LSTF, Station Blackout, Pump Seal LOCA, Accident Management Actions, Steam Generator, Primary Depressurization, Accumulator, Gas Inflow, ECCS

ROSA/LSTF 実験 TR-LF-15 データレポート
—ポンプシール冷却材喪失事故を伴う全交流電源喪失時のアクシデントマネジメント策—

日本原子力研究開発機構 安全研究・防災支援部門
安全研究センター 原子炉安全研究ディビジョン

竹田 武司

(2023 年 8 月 23 日受理)

ROSA-V 計画において、大型非定常実験装置 (LSTF) を用いた実験 (実験番号:TR-LF-15) が 2014 年 6 月 11 日に行われた。ROSA/LSTF TR-LF-15 実験では、加圧水型原子炉 (PWR) のポンプシール冷却材喪失事故 (LOCA) を伴う、補助給水機能喪失を特徴とする TMLB' のシナリオでの全交流電源喪失時のアクシデントマネジメント (AM) 策を模擬した。ポンプシール LOCA は、0.1% 低温側配管破断により模擬した。このとき、非常用炉心冷却系 (ECCS) である高圧注入系及び低圧注入系の全故障とともに、ECCS の蓄圧注入タンクから一次系への非凝縮性ガス (窒素ガス) の流入を仮定した。

蒸気発生器 (SG) 二次側水位が特定の低水位まで低下すると、一次系圧力は上昇に転じた。SG 二次側水位喪失後、加圧器の安全弁が周期的に開いたため、一次冷却材の喪失につながった。故に、高圧条件でボイルオフによる炉心露出が生じた。模擬燃料棒被覆管表面温度の 10K の上昇を確認した時点で、SG 二次側減圧を一番目の AM 策として開始した。この AM 策では、両 SG の安全弁を開放した。また、一番目の AM 策開始後少し遅れた時点で、加圧器の安全弁の開放による一次系減圧を二番目の AM 策として開始した。さらに、一番目の AM 策に従い SG 二次側圧力が 1.0 MPa に低下した時点で、低水頭ポンプによる給水ラインから両 SG 二次側への注水を三番目の AM 策として開始した。三番目の AM 策の開始直後、SG 二次系からの除熱が再開したため、一次系圧力の低下が促進された。蓄圧注入系から両低温側配管への冷却材注入による炉心水位の回復により、全炉心はクエンチした。窒素ガスが SG U 字管内に蓄積したため、一次系の減圧率は低下した。

本報告書は、ROSA/LSTF TR-LF-15 実験の手順、条件および実験で観察された主な結果をまとめたものである。

Contents

1.	Introduction	1
2.	Overview of LSTF	3
3.	Test Conditions and Procedures	4
3.1	Initial Steady State and Boundary Conditions	5
3.2	Test Procedures	6
3.3	Instrumentation	7
3.3.1	Measured Data	7
3.3.2	Data Conversion, Reduction, and Calibration	8
3.3.3	Data Qualification	8
4.	Experimental Results	13
4.1	Initial and Boundary Conditions	13
4.2	Thermal-hydraulic Responses Concerning Boundary Conditions	13
4.3	Transient Thermal-hydraulic Responses	14
4.3.1	Thermal-hydraulic Responses in Pressure Vessel	16
4.3.2	Thermal-hydraulic Responses in Primary Loops	19
4.3.3	Thermal-hydraulic Responses of Steam Generators	19
5.	Summary	52
	Acknowledgement	53
	References	53
	Appendix A Available Experimental Data List	55

目次

1. 緒言	1
2. LSTF の概要	3
3. 実験条件および手順	4
3.1 初期定常および境界条件	5
3.2 実験手順	6
3.3 計装	7
3.3.1 計測データ	7
3.3.2 データ変換、処理および校正	8
3.3.3 データ評価	8
4. 実験結果	13
4.1 初期および境界条件	13
4.2 境界条件に係る熱水力応答	13
4.3 過渡熱水力応答	14
4.3.1 圧力容器内の熱水力応答	16
4.3.2 一次系ループ内の熱水力応答	19
4.3.3 蒸気発生器の熱水力応答	19
5. 結言	52
謝辞	53
参考文献	53
付録 A 利用可能な実験データリスト	55

List of Tables

Table 3-1	Specified initial steady state and boundary conditions ··· ·..	9
Table 3-2	Specified control logic, operation set points, and conditions ··· ··· ··· ·..	11
Table 3-3	Specified pump rotation speed ratio ··· ·..	11
Table 3-4	Pre-determined core power decay curve ··· ·..	12
Table 4-1	Initial steady state conditions ··· ·..	22
Table 4-2	Chronology of major events until break valve closure ··· ·..	23
Table A-1	List of available experimental data for LSTF TR-LF-15 ··· ·..	56

List of Figures

Fig. 2-1	Schematic view of the Large Scale Test Facility (LSTF) ··· ··· ··· ·..	3
Fig. 3-1	Configuration of break unit ··· ·..	12
Fig. 4-1	Core power ··· ·..	24
Fig. 4-2	Pressurizer heater power ··· ·..	25
Fig. 4-3	Pressurizer liquid level (-200 to 1000 s) ··· ·..	25
Fig. 4-4	Primary coolant pump rotation speed ··· ·..	26
Fig. 4-5	Primary loop mass flow rate ··· ·..	26
Fig. 4-6	SG main steam flow rate ··· ·..	27
Fig. 4-7	SG main feedwater flow rate ··· ·..	27
Fig. 4-8	SG secondary-side collapsed liquid level ··· ·..	28
Fig. 4-9	Water injection flow rate into SG secondary-side via AFW pump ··· ·..	28
Fig. 4-10	Time-integrated break flow and break flow rate ··· ·..	29
Fig. 4-11	Liquid level in accumulator tank ··· ·..	29
Fig. 4-12	Coolant injection flow rate from accumulator tank ··· ·..	30
Fig. 4-13	Pressurizer liquid level (0 to 28000 s) ··· ·..	30
Fig. 4-14	Primary and secondary pressures (0 to 28000 s) ··· ·..	31
Fig. 4-15	Primary and secondary pressures (15000 to 19000 s) ··· ·..	31
Fig. 4-16	SG safety valve flow rate ··· ·..	32
Fig. 4-17	Upper plenum collapsed liquid level ··· ·..	32
Fig. 4-18	Core collapsed liquid level (0 to 28000 s) ··· ·..	33
Fig. 4-19	Core collapsed liquid level (14800 to 16400 s) ··· ·..	33
Fig. 4-20	Typical core exit temperatures (0 to 28000 s) ··· ·..	34
Fig. 4-21	Typical core exit temperatures (15000 to 15600 s) ··· ·..	34
Fig. 4-22	Core exit temperatures at center of UCP (15000 to 15600 s) ··· ·..	35
Fig. 4-23	Core exit temperatures at peripheral region of UCP (15000 to 15600 s) ··· ·..	35

Fig. 4-24	Core exit temperatures at outer region of UCP (15000 to 15600 s)	36
Fig. 4-25	Typical cladding surface temperatures at Positions 9-5 (0 to 28000 s)	36
Fig. 4-26	Typical cladding surface temperatures at Positions 4-1 (0 to 28000 s)	37
Fig. 4-27	Typical cladding surface temperatures at Positions 9-5 (14800 to 16400 s) ..	37
Fig. 4-28	Typical cladding surface temperatures at Positions 4-1 (14800 to 16400 s) ..	38
Fig. 4-29	Cladding surface temperatures at Position 9 (14800 to 16400 s)	38
Fig. 4-30	Cladding surface temperatures at Position 8 (14800 to 16400 s)	39
Fig. 4-31	Cladding surface temperatures at Position 7 (14800 to 16400 s)	39
Fig. 4-32	Cladding surface temperatures at Position 6 (14800 to 16400 s)	40
Fig. 4-33	Cladding surface temperatures at Position 5 (14800 to 16400 s)	40
Fig. 4-34	Cladding surface temperatures at Position 4 (14800 to 16400 s)	41
Fig. 4-35	Cladding surface temperatures at Position 3 (14800 to 16400 s)	41
Fig. 4-36	Downcomer collapsed liquid level	42
Fig. 4-37	Upper-head collapsed liquid level	42
Fig. 4-38	Hot leg liquid level	43
Fig. 4-39	Hot leg fluid temperature	43
Fig. 4-40	Cold leg liquid level	44
Fig. 4-41	Cold leg fluid temperature	44
Fig. 4-42	Crossover leg downflow-side collapsed liquid level	45
Fig. 4-43	Crossover leg upflow-side collapsed liquid level	45
Fig. 4-44	SG U-tube upflow-side collapsed liquid level in loop with pressurizer	46
Fig. 4-45	SG U-tube downflow-side collapsed liquid level in loop with pressurizer ..	46
Fig. 4-46	SG U-tube upflow-side collapsed liquid level in loop without pressurizer ..	47
Fig. 4-47	SG U-tube downflow-side collapsed liquid level in loop without pressurizer ..	47
Fig. 4-48	SG U-tube downflow-side fluid temperature in loop with pressurizer	48
Fig. 4-49	SG U-tube downflow-side fluid temperature in loop without pressurizer ..	48
Fig. 4-50	Nitrogen gas mole fraction of SG U-tube in loop with pressurizer	49
Fig. 4-51	Nitrogen gas mole fraction of SG U-tube in loop without pressurizer	49
Fig. 4-52	SG inlet plenum collapsed liquid level	50
Fig. 4-53	SG secondary-side fluid temperature in loop with pressurizer	51
Fig. 4-54	SG secondary-side fluid temperature in loop without pressurizer	51

Acronyms and Abbreviations

AC	Alternating Current
ACC	Accumulator
CET	Core Exit Temperature
AFW	Auxiliary Feedwater
AM	Accident Management
ATLAS	Advanced Thermal-hydraulic Test Loop for Accident Simulation
ECCS	Emergency Core Cooling System
LOCA	Loss-of-coolant Accident
LSTF	Large Scale Test Facility
NEA	Nuclear Energy Agency
OECD	Organisation for Economic Co-operation and Development
PWR	Pressurized Water Reactor
PZR	Pressurizer
ROSA	Rig-of-Safety Assessment
SBO	Station Blackout
SG	Steam Generator
TMLB'	T (transient event) M (failure of secondary system relief valves and power conversion system) L (failure of secondary system relief valves and auxiliary feedwater system) B' (failure to recover either on-site or off-site electric power within about 1-3 h following initiating transient which is loss of off-site AC power)
UCP	Upper Core Plate

This is a blank page.

1. Introduction

Some experimental investigations [1]-[3] have been performed for a station blackout (SBO) transient with TMLB' scenario [4] in a pressurized water reactor (PWR). These tests utilized the Large Scale Test Facility (LSTF) [5] in the Rig-of-Safety Assessment-V (ROSA-V) Program. The LSTF simulates a Westinghouse-type four-loop 3423 MW (thermal) PWR by a full-height and 1/48 volumetrically-scaled two-loop system. The TMLB' scenario involves prolonged complete loss of AC power, unavailability of turbine-driven auxiliary feedwater (AFW), and malfunction of relief valves in primary and steam generator (SG) secondary-side systems. The AC power includes the off-site power and the on-site emergency diesel generator power.

An LSTF experiment denoted as TR-LF-15 was carried out on June 11, 2014, simulating accident management (AM) actions during a PWR SBO transient with the TMLB' scenario with pump seal loss-of-coolant accident (LOCA). The TR-LF-15 test also focuses on effects of the pump seal LOCA on the primary pressure, core uncover, etc. during the SBO transient.

In the new regulatory requirements in Japan, the SBO transient with the pump seal LOCA was postulated as one of events, which should be evaluated the effectiveness of measures against core damage [6]. The primary coolant pump is equipped with multistage shaft seals to avoid leakage of primary coolant from the shaft. Cold seal water is injected into the front of the 1st stage shaft seal closest to the impeller exploiting a seal water injection pump. This prevents the hot primary coolant from reaching the pump seals directly during the normal operation. When SBO happens, the seal water injection pump stops, thereby causing that the hot primary coolant may attain the pump seals. The primary coolant pump seals may thus be damaged because they become hot. This would give rise to the pump seal LOCA (i.e., loss of primary coolant from the pump seals). Meanwhile, attempts have been made to reduce leakage from the pump seals in the SBO sequence by deploying passive thermal shutdown seals for the primary coolant pump [7]-[9].

A 0.1% cold leg break was made to simulate the pump seal LOCA [10]. The experiment assumed total failure of both high pressure injection system and low pressure injection system of emergency core cooling system (ECCS). Additionally, non-condensable gas (nitrogen gas) ingress to the primary system from accumulator (ACC) tanks of ECCS was supposed. When a rise of 10 K was confirmed in cladding surface temperature of simulated fuel rods during core uncover, SG secondary-side depressurization was launched as the first AM action. This SG secondary-side depressurization was done by fully opening the safety valves in both SGs. Primary depressurization was taken by completely opening the safety valve of a pressurizer (PZR) as the second AM action with some delay after the first AM action onset. When the SG secondary-side pressure dropped to 1.0 MPa following the first AM action, water was injected into the secondary-side of both SGs through feedwater lines employing low-head pumps as

the third AM action.

The TR-LF-15 test objectives were as follows; (i) to elucidate thermal-hydraulic phenomena involved, (ii) to clarify the AM actions effectiveness for both core cooling and primary depressurization, and (iii) to provide experimental data for the assessment of thermal-hydraulic safety analysis computer codes. The LSTF test data would be useful to define the conditions of counterpart testing by means of other integral test facilities, such as ATLAS (Advanced Thermal-hydraulic Test Loop for Accident Simulation) [11]. The aim of the counterpart testing is to address scaling problems through thermal-hydraulic phenomena. In this regard, Japan Atomic Energy Agency have provided the LSTF test data on a 1% small-break LOCA at the top of a pressure vessel with AM actions and nitrogen gas inflow [12] for the counterpart testing in the ATLAS-related OECD/NEA Project.

This report summarizes the test procedures, conditions, and major observations in the ROSA/LSTF experiment TR-LF-15. All the experimental data were processed carefully and qualified to acquire the best possible accuracy.

2. Overview of LSTF

Figure 2-1 shows a schematic view of the LSTF that simulates a typical 3423 MW (thermal) four-loop Westinghouse-type PWR with a two-loop system model by full height and 1/48 in volume [5]. The reference PWR of the LSTF is Tsuruga Unit-2 of Japan Atomic Power Company. The LSTF is composed of a pressure vessel, PZR, and primary loops. Each loop includes an active SG, primary coolant pump, crossover leg, hot leg, and cold leg. The crossover leg is a primary piping that connects the primary coolant pump to the SG. Loops with and without PZR are designated as loop-A and loop-B, respectively. The hot leg and cold leg, 207 mm in inner-diameter each, are sized to conserve the volumetric scale (2/48) and the ratio of length to square root of pipe diameter to better simulate flow regime transitions in the primary loops [13]. Each SG is furnished with 141 full-size U-tubes (inner-diameter of 19.6 mm each), inlet and outlet plena, boiler section, steam separator, steam dome, steam dryer, main steam line, four downcomer pipes, and other internals (see pp.260-273 in Ref. [5]). Six U-tubes are instrumented for each SG. Tubes 1 and 6 are short tubes (Type 1; see p.267 in Ref. [5]), Tubes 2 and 5 are medium tubes (Type 5), and Tubes 3 and 4 are long tubes (Type 9). The LSTF represents the reference PWR bypasses involving eight upper-head spray nozzles (inner-diameter of 3.4 mm each) (see p.202 in Ref. [5]) and the hot leg nozzle (see p.196 in Ref. [5]) leakage. The spray nozzles allow bypass flow that amounts to 0.3% of the total core flow rate during the initial steady state, while bypass area of the hot leg nozzle is set to allow 0.2% bypass flow for each loop. The LSTF core, 3.66 m in active height, mainly consists of 1008 electrically heater rods in 24 rod bundles to simulate the fuel rod assembly and 96 non-heating tie rods to simulate control rod guide thimble (see p.220 in Ref. [5]). The angle of the PZR surge line to the hot leg is 45°. All the types of ECCS fitted to the reference PWR are installed in the LSTF. Nitrogen gas is used for pressurization of ACC tanks of ECCS.

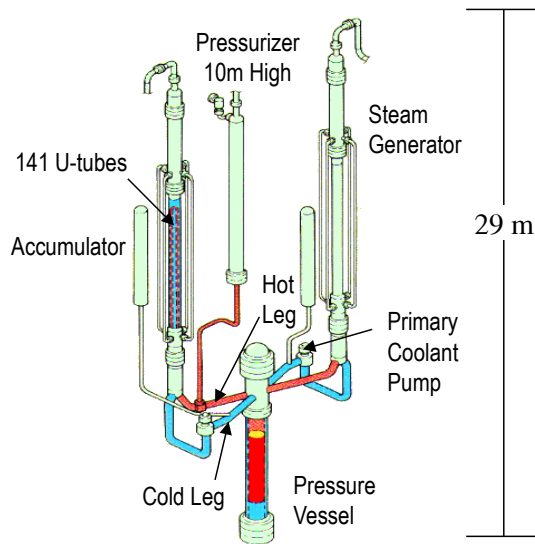


Fig. 2-1 Schematic view of the Large Scale Test Facility (LSTF)

3. Test Conditions and Procedures

With respect to the break, ECCS, and control logic, following assumptions were posed to the TR-LF-15 test conditions.

The assumption related to the break for simulating the pump seal LOCA is the following;

- 1) Break size (flow area) corresponds to 0.1% of the volumetrically-scaled (1/48) cross-sectional area of the reference PWR cold leg. As presented in **Fig. 3-1**, the break is simulated by using a 3.2 mm inner-diameter sharp-edge orifice. The break orifice is fixed at the downstream of a horizontal pipe. This pipe is connected to a vertical pipe attached to a cold leg break nozzle placed at the top of a cold leg in loop without PZR.

The assumptions concerning the ECCS are as follows;

- 2) Total failure of both high pressure injection system and low pressure injection system
- 3) When the primary pressure reduces to 4.51 MPa, ACC system is actuated in both loops. Coolant is injected from the ACC system into both cold legs. The ACC coolant injection flow rate ratio of loop with PZR to loop without PZR is designed to become 1:1. The ACC coolant injection temperature is 320 K.
- 4) For each loop, non-condensable gas (nitrogen gas) inflow to the primary system from the ACC tank takes place owing to failure of the ACC system isolation after the ACC coolant injection initiation.

The assumptions regarding the control logic are as below;

- 5) Relief valves in the primary and SG secondary-side systems are unavailable.
- 6) A scram signal is generated at time zero, causing closure of SG main steam stop valve, termination of SG main feedwater, and manual closure of SG main steam isolation valves.
- 7) When an increase of 10 K is confirmed in cladding surface temperature of simulated fuel rods during core uncover, SG secondary-side depressurization is started as the first AM action. In this SG secondary-side depressurization, the safety valves in both SGs are fully opened because the relief valves in both SGs are unable to use.
- 8) Primary depressurization is initiated by completely opening the safety valve of PZR as the second AM action with some delay after the first AM action onset. This is because the relief valve of PZR cannot be utilized.
- 9) When the SG secondary-side pressure lowers to 1.0 MPa through the first AM action, water is injected into the secondary-side of both SGs via feedwater lines exploiting low-head pumps as the third AM action. In this test, AFW pump in the SG secondary-side system is employed as an alternative for the low-head pump. The water injection flow rate into each SG secondary-side is fixed to about 0.75 kg/s until the SG secondary-side collapsed liquid level achieves around 12 m. The water injection flow rate into each SG secondary-side is controlled to keep the SG secondary-side collapsed liquid level at around 12 m thereafter.

The water injection temperature into each SG secondary-side is 310 K.

- 10) Thresholds of maximum cladding surface temperature for the LSTF core protection system are as follows;
 $958\text{K}=70\%$, $961\text{K}=35\%$, $966\text{K}=13\%$, $977\text{K}=5\%$, $1003\text{K}=0\%$, of pre-determined value.

3.1 Initial Steady State and Boundary Conditions

The specified initial steady state and boundary conditions are listed in **Table 3-1**. Initial steady state conditions such as PZR pressure, fluid temperatures in the hot leg and cold leg were 15.6 MPa, 598 K and 563 K respectively (to be indicated in **Table 4-1**), according to the reference PWR conditions.

The LSTF initial core power is limited to 10 MW, on account of a limitation in the capacity of power supply. The 10 MW power corresponds to 14% of the volumetrically-scaled (1/48) PWR nominal core power (3423 MW). Radial peaking factor for all high-, mean-, and low-power rod bundles is 1.00 in "Case 1" (see p.228 in Ref. [5]) shown in **Table 3-1**. Namely, the radial core power profile is flat. Axial core power profile is a 9-step chopped cosine with a peaking factor of 1.495 (see p.227 in Ref. [5]). To attain the prototypical initial fluid temperatures with this core power, core flow rate was set to 14% of the 1/48-scaled nominal flow rate. Initial SG secondary-side pressure was raised to 7.3 MPa to limit the primary-to-secondary heat transfer rate to 10 MW, while 6.1 MPa is nominal value in the reference PWR. Initial PZR liquid level was about 7.4 m that is equivalent to about 66% of the PZR vessel height (see p.396 in Ref. [5]). Initial SG secondary-side collapsed liquid level was about 10.2 m that corresponds to the SG medium tube height.

Backup heaters in the PZR mitigate system heat losses. Power of the PZR backup heaters was 33.8 kW as the initial condition. The PZR backup heater power turned off when the PZR liquid level became below 2.3 m. Many regions of the LSTF are provided with trace heaters to mitigate environmental heat losses.

The configuration of the break unit is drawn in **Fig. 3-1**. The break was simulated by utilizing a 3.2 mm inner-diameter sharp-edge orifice No.1 (see p.307 in Ref. [5]). The orifice was mounted at the downstream of a horizontal pipe (inner-diameter of 87.3 mm). This pipe was joined to a vertical pipe (inner-diameter of 87.3 mm) fitted to a cold leg break nozzle (N-7i; see p.96 and pp.239-240 in Ref. [5]) positioned at the top of a cold leg in loop without PZR. The orifice flow area was consistent with 0.1% of the 1/48-scaled cross-sectional area of the reference PWR cold leg. Venturi flow meter (FE-570-BU; see p.303 in Ref. [5]) was installed in the break unit for the purpose of qualitatively monitoring the break flow rate during the test.

For controlling ACC water injection volume (see p.322 in Ref. [5]), the specified initial water level and volume above the standpipe were 1.58 m and 1.12 m^3 respectively for both loops.

The specified initial volume of non-condensable gas (nitrogen gas) in the ACC tank was 0.46 m³ for both loops. The angle of the coolant injection from the ACC tank into the cold leg via the ECCS nozzle (N-14a or N-14b; see p.83 and pp.239-240 in Ref. [5]) is 90° for loop with PZR (loop-A) and 45° for loop without PZR (loop-B) (see pp.397-398 in Ref. [5]).

3.2 Test Procedures

Table 3-2 shows the specified control logic, operation set points, and conditions. The experiment was launched at time zero by opening a break valve located downstream of the break orifice at the cold leg in loop without PZR, as well as the generation of a scram signal.

Table 3-3 shows the specified rotation speed ratio of primary coolant pump. Simultaneously with the break, the rotation speed of primary coolant pumps was raised up to about 1470 rpm in 4 s. This better simulates pressure and temperature transients in the reference PWR. The specified pump rotation speed was decreased to zero at 268 s (i.e., 250 s after the initiation of the pump coastdown at 18 s).

A scram signal was generated at time zero. This caused the closure of the SG main steam stop valve, the termination of the SG main feedwater, and the manual closure of the SG main steam isolation valves. **Table 3-4** shows the pre-determined core power decay curve. The core power decay curve was defined by adding heat losses to the calculation result of the core power with the RELAP5 code considering delayed neutron fission power and stored heat in PWR fuel rod [14]. The core power was held at the initial value of 10 MW for 18 s until the scaled PWR core decay power dropped to 10 MW. The LSTF core power began a decay afterwards according to the specified core power.

In this test, the (existing) relief valve of PZR was exploited as an alternative for the safety valve of PZR. Therefore, the PZR safety valve was simulated by employing a 6.83 mm inner-diameter sharp-edge orifice. Set point pressures for opening and closure of the simulated PZR safety valve were 17.26 MPa and 17.06 MPa respectively, referring to the corresponding pressures for the PZR safety valve in the reference PWR.

In this test, the (existing) relief valves in both SGs were used as an alternative for the safety valves in both SGs. Hence, the SG safety valve was simulated by utilizing a 16.2 mm inner-diameter sharp-edge orifice. Set point pressures for opening and closure of the simulated SG safety valves were 8.68 MPa and 7.69 MPa respectively, by reference to the corresponding pressures for the SG safety valves in the reference PWR.

The ACC system is activated in both loops at the primary pressure of 4.51 MPa according to the reference PWR. The ACC coolant injection flow rate ratio of loop with PZR to loop without PZR was intended to become 1:1 (to be plotted in **Fig. 4-12**). The ACC coolant injection

temperature is 320 K, which is the same as that in the reference PWR.

Relating to the third AM action, water was injected into the secondary-side of both SGs through feedwater lines at the SG secondary-side pressure of 1.0 MPa. The water injection exploited the (existing) AFW pump in the SG secondary-side system as an alternative for low-head pump. The operator manually injected water into each SG secondary-side by monitoring the narrow-range (0-1 kg/s) feedwater flow rate [Tag Name; FE520B-PAA (for secondary-side of SG in loop with PZR), FE530B-PAB (for secondary-side of SG in loop without PZR)] (see pp.257-258 in Ref. [5]). The water injection flow rate into each SG secondary-side was set to about 0.75 kg/s until the SG secondary-side collapsed liquid level reached around 12 m (to be set out in **Fig. 4-9**). This value of about 0.75 kg/s was nearly equivalent to the volumetrically-scaled AFW flow rate of the reference PWR. The water injection flow rate into each SG secondary-side was regulated to maintain the SG secondary-side collapsed liquid level at around 12 m thereafter. The water injection temperature into each SG secondary-side was 310 K, which was the same as the AFW injection temperature in the reference PWR.

3.3 Instrumentation

Instruments are equipped in the LSTF to understand and evaluate thermal-hydraulic responses during simulated accidents and transients.

3.3.1 Measured Data

A list of available experimental data is shown in **Table A-1**, which is composed of Sequential No., Function ID., Tag Name, measurement location, range, unit, and uncertainty. The Tag Name is a fixed naming unique to each measurement. The alphabetical prefix in the Function ID. and Tag Name represents the kind of variable or the kind of measurement as follows;

- TE, fluid temperature,
- DT, differential temperature,
- TW, heater rod and structure temperature,
- FE, flow rate measured with conventional (differential pressure) flow meters,
- PE, pressure,
- MI, miscellaneous instrumented-signal (power, pump rotation speed, etc.),
- LE, liquid level,
- DP, differential pressure,
- DE, fluid density measured with gamma-ray densitometer.

After the experiment, data from these measurements are processed to obtain the “secondary” data, such as area-averaged fluid density derived from measurement with three-beam gamma-

ray densitometer. These data are stored with Function ID. starting with a prefix of “RC”. The measurement uncertainty is assessed according to the accuracy of the relevant instrument.

3.3.2 Data Conversion, Reduction, and Calibration

The instrumented-signals are recorded in volts by the data logger of DARWIN system (Yokogawa Electric Co.), and are converted into engineering units utilizing appropriate conversion equations and factors. Differential pressure (DP) cell is a device that measures the differential pressure between two inputs. Some parameters such as flow rate (FE) and liquid level (LE) that employ DP cell data require the calculation of the single-phase coolant density based on local pressure and fluid temperature data using steam table.

DP cell data for both the differential pressures and liquid levels are corrected on the basis of a similar calibration test for static pressure effect, which is performed separately. Three-valve manifold is operated for each of DP cells to obtain zero calibration data for 200 s twice at a little before the break valve opening and at a little after the closure of the break valve.

The applicability of flow rates measured with the conventional flow meters employing venturi, orifice or nozzle and DP cell is limited in principle to either single-phase liquid or vapor flow. In addition, the accuracy is poor when the readings are below about 20% of the measurement range. This is explained by the fact that the flow rate is proportional to the square root of the measured DP. For example, a zero level drift of 1% in the DP cell output may result in the flow rate reading of 10% of the measurement range especially when the actual flow rate is nearly equal to zero. It is thus good to pay attention when the flow rate is below about 20% of the measurement range even though the data are corrected based on a calibration test for static pressure effect.

Two-phase flow instruments, such as gamma-ray densitometers, use certain conversion equations considering attenuation effects of gamma-ray that goes through coolant flow.

After the data acquisition, some experimental data are calibrated. The high-range pressure data in the PZR and the upper plenum, for example, are corrected on the basis of a zero level shift using the low-range pressure data first, and then all the density data are calibrated at two points with different fluid conditions.

3.3.3 Data Qualification

The experimental data are qualified manually. Thermocouple data are reviewed by employing pre-test ambient temperature data for anomalous readings, and are mutually compared with readings of instruments in the same vicinity. Pressure transducers are checked for zero level drift as well as any other suspicious behaviors. The outputs of conductance probe, power meters, pump speed and vibration meters, and valve position indicators are individually

reviewed for inconsistent readings.

The flow meters, DP transducers, gamma-ray densitometers, and drag disk transducers require extensive manual qualification efforts. The validity of the flow meters and differential pressure data mostly depends on whether the reading is in the sensitive range of the measurement or not. The data from these instruments are presented with appropriate corrections based on calibration data for each transducer.

Available experimental data are “Good” defined as follows. “Good” means that the type of data has been reviewed manually, and is presumed to lie within the range and uncertainty values of the instruments based on the design specification which are published in the reference [5]. However, certain measurements may be affected by various extraneous factors such as flow velocity, flow regime, and wall effects. **Table A-1** shows the list of available experimental data qualified as “Good” for LSTF TR-LF-15 (Run ID named to be LFF).

Table 3-1 Specified initial steady state and boundary conditions (1/2)

Core	Initial core power	10 MW
	Radial core power profile	Case 1 (i.e., flat)
	Axial core power profile	9-step chopped cosine, peaking factor = 1.495
Primary Loops	Initial hot leg fluid temperatures	598.1 K
	Initial cold leg fluid temperatures	562.4 K
	Initial mass flow rate	24.3 kg/s / loop
	Initial downcomer-to-hot leg bypass	0.049 kg/s / loop
Pressurizer (PZR)	Initial pressure	15.5 MPa
	Initial liquid level	7.2 m
	Inner-diameter of safety valve orifice	6.83 mm
	Safety valve open / closure	Primary pressure = 17.26 / 17.06 MPa
Steam Generators (SGs)	Initial secondary-side pressure	7.3 MPa
	Initial secondary-side liquid level	10.3 m
	Initial main steam flow rate	2.74 kg/s
	Initial main feedwater flow rate	2.74 kg/s
	Main feedwater temperature	495.2 K
	Inner-diameter of safety valve orifice	16.2 mm
	Safety valve open / closure	SG secondary-side pressure = 8.68 / 7.69 MPa

Table 3-1 Specified initial steady state and boundary conditions (2/2)

Break

Location	Cold leg in loop without PZR (see Fig. 3-1)
Type	Sharp-edge orifice
Inner-diameter of orifice	3.2 mm

ECCS

High pressure injection system		Not actuated
Accumulator (ACC) system	Initiation of system	Primary pressure = 4.51 MPa
	Water temperature	320 K
	Initial water level above tank bottom in both loops	6.8 m
	Standpipe level above tank bottom in both loops	5.22 m
	Initial water volume above standpipe in both loops	1.12 m ³ *
	Initial gas volume in both loops	0.46 m ³
	Cross-sectional flow area above standpipe	0.7085 m ²
	Orifice diameter (d) in loops with / without PZR	38.2 mm / 35.0 mm
	Connecting pipe diameter (D) in both loops	97.1 mm
	Contraction ratio (d/D) in loops with / without PZR	0.393 / 0.360
Coolant injection flow rate ratio of loop with PZR to loop without PZR		1:1
Injection location		Cold legs in both loops
Low pressure injection system		Not actuated

$$* (6.8 - 5.22 [m]) \times 0.7085 [m^2] \approx 1.12 [m^3]$$

LSTF Core Protection System Logic

Control of core power to	Maximum cladding surface temperature reaches
70%	958 K
35%	961 K
13%	966 K
5%	977 K
0% (core power trip)	1003 K

Table 3-2 Specified control logic, operation set points, and conditions

Event	Condition
Break	Time zero
Generation of scram signal	Time zero
Initiation of primary coolant pump rotation speed simulation	Time zero
Initiation of core power decay curve simulation	Generation of scram signal
Closure of SG main steam stop valve	Generation of scram signal
Manual closure of SG main steam isolation valves	Generation of scram signal
Termination of SG main feedwater	Generation of scram signal
PZR backup heater off	PZR liquid level < 2.3 m
Initiation of SG secondary-side depressurization by fully opening safety valves in both SGs as first AM action	Confirmation of cladding surface temperature rise of 10 K during core uncover
Initiation of primary depressurization by completely opening safety valve of PZR as second AM action	Some delay after first AM action onset
Initiation of water injection into secondary-side of both SGs via feedwater lines as third AM action	SG secondary-side pressure = 1.0 MPa
Initiation of ACC system in both loops	Primary pressure = 4.51 MPa

Table 3-3 Specified pump rotation speed ratio

Time (s)	Rotation speed ratio	Time (s)	Rotation speed ratio	Time (s)	Rotation speed ratio
0	0.550	38	0.370	98	0.125
4	1.000	48	0.280	108	0.110
18	1.000	58	0.220	118	0.100
20	0.850	68	0.185	268	0.000
23	0.730	78	0.160		
28	0.540	88	0.140		

Table 3-4 Pre-determined core power decay curve

Time (s)	Power (MW)	Time (s)	Power (MW)	Time (s)	Power (MW)
0	10	150	2.589	2000	1.404
18	10	200	2.429	3000	1.262
20	8.316	300	2.246	4000	1.169
30	5.532	400	2.166	5000	1.103
40	4.670	500	2.079	6000	1.052
50	4.072	600	1.998	8000	0.980
60	3.704	800	1.743	10000	0.929
80	3.209	1000	1.653	20000	0.795
100	2.929	1500	1.508	50000	0.657

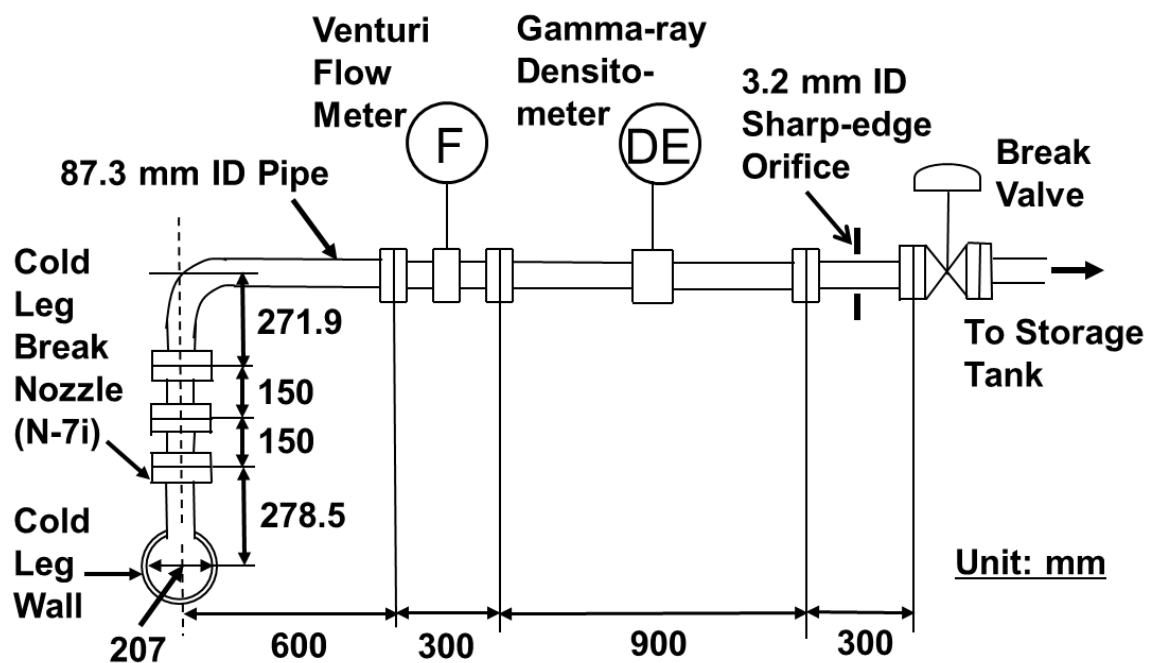


Fig. 3-1 Configuration of break unit

4. Experimental Results

4.1 Initial and Boundary Conditions

Initial steady state conditions achieved in the experiment were in reasonable agreement with the specified values, as mentioned in **Table 4-1**. The measured values indicated are those averaged for the last 60 s prior to the onset of the break. Initial SG re-circulation ratio estimated from the measured flow rates in the downcomer and SG main steam line was 6.5 in loop with PZR (loop-A) and 6.3 in loop without PZR (loop-B). **Table 4-2** shows the chronology of major events until 28833 s when the break valve was closed.

4.2 Thermal-hydraulic Responses Concerning Boundary Conditions

As presented in **Fig. 4-1**, the core power began to decay at 20 s. The core power was controlled to the pre-determined value until 28818 s when the core power turned off. This is because the peak cladding temperature of 790 K was below the pre-determined threshold of 958 K for the LSTF core protection system (to be depicted in **Figs. 4-25 through 4-28**).

As noted in **Fig. 4-2**, the power value of the PZR backup heaters was initially kept constant at 33.8 kW. The PZR backup heater power turned off by 529 s because the PZR liquid level became below 2.3 m (as set out in **Fig. 4-3**). The PZR liquid level degraded immediately and monotonously after the break. The PZR became voided by 760 s.

Figures 4-4 and 4-5 show the primary coolant pump rotation speed and the primary loop mass flow rate measured by using a venturi flow meter at each primary coolant pump suction leg, respectively. The pump rotation speed started an increase simultaneously with the break, and attained about 1470 rpm in 4 s. The pump coastdown initiated at 19 s. The pump rotation speed reduced thereafter, which led to a decrease in the primary loop mass flow rate. Single-phase natural circulation continued until liquid levels formed in hot legs (to be plotted in **Fig. 4-38**) after the primary coolant pumps stopped. When the primary loop mass flow rate became zero, natural circulation mode changed from two-phase natural circulation into reflux condensation. The primary loop mass flow rate oscillated during the time period of the coolant injection from the ACC system into both cold legs (to be presented in **Fig. 4-12**).

Figures 4-6 and 4-7 show the SG main steam and feedwater flow rates, respectively. The SG main steam was terminated by the closure of the SG main steam stop valve [Valve No.; AOV (air-operated valve) -220] (see p.113 in Ref. [5]) at 1 s, following the scram signal. The main feedwater injection into the secondary-side of both SGs was terminated by the closure of the SG main feedwater line valve [Valve No.; AOV-260] (see p.113 in Ref. [5]) at 2 s. The main steam isolation valves of both SGs [Valve No.; AOV-170 and AOV-200] (see pp.111-112 in Ref. [5]) were manually closed at 3 s.

Figures 4-8 and 4-9 show the SG secondary-side collapsed liquid level and water injection flow rate into the SG secondary-side through the feedwater line via alternative utilization of the AFW pump in the SG secondary-side system, respectively. The SG secondary-side liquid level began to rise after the main steam stop valve closure and the main feedwater termination (**Figs. 4-6 and 4-7**). This seems to be attributed to the decrease in the net upward steam flow through the SG boiling section. The SG secondary-side liquid level gradually dropped with some fluctuation owing to cycle opening of the SG safety valves (to be indicated in **Fig. 4-16**). The SG secondary-side liquid level became lost by 8130 s. The water injection into the secondary-side of both SGs was started as the third AM action at 15360 s, and continued thereafter. The liquid level recovered in the SG secondary-side at 15500 s, which resulted in the resumption of the heat removal from the SG secondary-side system. During the time period other than the operation of the AFW pump, flow meter (see pp.257-258 in Ref. [5]) for water counts flow rate in the return line from the AFW pump to the refueling water storage tank. The SG secondary-side liquid level reached around 12 m at 22090 s. Until then the water injection flow rate into the SG secondary-side was about 0.74-0.80 kg/s in loop with PZR and about 0.72-0.78 kg/s in loop without PZR. The water injection flow rate into each SG secondary-side was adjusted to hold the SG secondary-side liquid level at around 12 m thereafter.

Figure 4-10 shows the time-integrated break flow evaluated from the liquid level increase in the storage tank, and the break flow rate derived as the differential of the time-integrated break flow. The break flow rate reduced roughly stepwise. The break flow turned from single-phase liquid to two-phase flow at around 1500 s when liquid levels formed in cold legs (to be depicted in **Fig. 4-40**). The break flow rate increased with the liquid level recovery in the cold legs by coolant from the ACC system (to be mentioned in **Fig. 4-12**). The break flow changed to single-phase vapor at around 20000 s when the cold legs became empty of liquid.

Figure 4-11 shows the liquid level in the ACC tank. **Figure 4-12** gives the coolant injection flow rate from the ACC tank derived from the liquid level history in the ACC tank. Another name for the ACC tank in loop with PZR is ACC-cold tank, while that for the ACC tank in loop without PZR is ACC-hot tank. The coolant injection temperature is 320 K in both the ACC-cold tank and ACC-hot tank, but the heater capacity of the ACC-hot tank is designed to be twice that of the ACC-cold tank. When the primary pressure lowered to 4.51 MPa, the ACC system initiated in both loops at 16210 s. The initial water level above the ACC tank bottom was 6.84 m in both loops. The final water level above the ACC tank bottom was 5.31 m in loop with PZR and 5.29 m in loop without PZR. When the primary pressure dropped to about 1.6 MPa, the ACC system terminated in both loops at 17370 s.

4.3 Transient Thermal-hydraulic Responses

Figure 4-13 shows the PZR liquid level. A monotonous decline in the PZR liquid level started

soon after the break. The PZR once became voided at 760 s. The PZR liquid level recovered with an increase in the primary pressure at 9250 s (to be plotted in **Fig. 4-14**). The PZR liquid level largely rose following periodic opening of the PZR safety valve (to be noted in **Fig. 4-14**), and achieved 10.3 m at 14350 s. The PZR liquid level reduced after the SG inlet plenum became empty of liquid (to be mentioned in **Fig. 4-52**). A steep depression began in the PZR liquid level at 15040 s with the primary depressurization through the complete opening of the PZR safety valve. The PZR liquid level became lost again at 17020 s.

Figures 4-14 and 4-15 show the primary and secondary pressures. The primary pressure initiated a decrease at time zero when the break valve was opened. Very small size of break brought about a slow primary depressurization. The SG secondary-side pressure rapidly raised up to about 8.7 MPa after the closure of the SG main steam isolation valve. **Figure 4-16** shows the flow rate of the SG safety valve that uses the SG relief valve as an alternative. The SG secondary-side pressure fluctuated between 8.68 MPa and 7.69 MPa by cycle opening of the SG safety valves during the time period of around 190-8120 s. The primary pressure once became close to the SG secondary-side pressure. When the SG secondary-side liquid level dropped to about 3 m (**Fig. 4-8**), the primary pressure turned to increase at around 4750 s. This was due to deterioration in the heat removal from the SG secondary-side system. The primary pressure fluctuated between 17.26 MPa and 17.06 MPa because the PZR safety valve periodically opened during the time period of around 13680-15030 s. Loss of primary coolant along with cycle opening of the PZR safety valve induced core uncovering at high pressure (to be depicted in **Figs. 4-25 through 4-28**). When the cladding surface temperature increase of 10 K was confirmed during the core uncovering, SG secondary-side depressurization was taken as the first AM action at 15020 s (**Fig. 4-16**). This SG secondary-side depressurization was made by fully opening the safety valves in both SGs. Primary depressurization was started by completely opening the PZR safety valve as the second AM action at 15040 s. The SG secondary-side and primary pressures considerably decreased immediately after the first and second AM actions, respectively. When the SG secondary-side pressure lowered to 1.0 MPa following the first AM action, water was injected into the secondary-side of both SGs as the third AM action at 15360 s. Just after that, the heat removal from the SG secondary-side system resumed because of the liquid level recovery in the SG secondary-side. Therefore, a reduction in the primary pressure was accelerated. The SG secondary-side pressure once rose, and then declined being followed by the primary pressure decrease. When the primary pressure dropped to 4.51 MPa, the ACC system initiated in both loops at 16210 s (**Fig. 4-12**). When the primary pressure lowered to about 1.6 MPa, the ACC system terminated in both loops at 17370 s. As indicated in **Fig. 4-15**, the primary depressurization rate reduced after around 18200 s. This is because the nitrogen gas accumulated in the SG U-tubes (to be described in **Section 4.3.3**). The nitrogen gas accumulation implies degradation in the

condensation heat transfer in the SG U-tubes. The primary and SG secondary-side pressures were about 1.2 MPa and about 0.6 MPa respectively at 28000 s (**Fig. 4-14**).

4.3.1 Thermal-hydraulic Responses in Pressure Vessel

Liquid level behaviors in upper plenum and core

Figure 4-17 shows the upper plenum collapsed liquid level. The upper plenum liquid level changed in response to the hot leg liquid level (to be presented in **Fig. 4-38**). **Figures 4-18 and 4-19** show the core collapsed liquid level. A significant depression started in the core liquid level at 14800 s after the upper plenum was emptied of liquid. Core uncover occurred by core boil-off at high pressure at 14950 s (to be noted in **Figs. 4-25 through 4-28**). The liquid level recovered in the core by coolant from the PZR at around 15600 s (**Fig. 4-13**). The core liquid level abruptly increased following the actuation of the ACC system at 16210 s (**Fig. 4-12**). The liquid level recovered in the upper plenum at around 16400 s.

Responses of core exit temperature (CET) and cladding surface temperature of simulated fuel rods

Figures 4-20 and 4-21 show the typical CETs at the center [Tag Name; TE-EX040-B21-UCP, -B24-UCP], peripheral region [TE-EX040-B18-UCP, -B19-UCP], and outer region [TE-EX040-B07-UCP, -B08-UCP] of upper core plate (UCP). The representative CETs account for the first and second highest CETs at each region of UCP. Thickness of UCP is 76.2 mm. The core exit thermocouples are installed 13 mm above the upper surface of UCP. The vertical and radial measurement positions of the CETs are presented in Ref. [5] (pp.377-378) and Ref. [5] (pp.385-386), respectively. The CETs were maintained saturated until 15150 s even after core uncover began partly at 14950 s (to be set out in **Figs. 4-25 through 4-28**). This was ascribed to condensate falling from hot leg nozzles (see p.196 in Ref. [5]). Subsequently, the CETs started to rise. The peak CET of 735 K was seen at the center [TE-EX040-B21-UCP] of UCP located above the B21 rod bundle at 15515 s. At that time, the CETs at the peripheral region of UCP were higher than those at the outer region of UCP. The CETs were kept saturated again after around 15600 s.

Figures 4-22, 4-23, and 4-24 show the distributions of the CETs at the center, peripheral region, and outer region of UCP, respectively. As for the CETs at the center of UCP (**Fig. 4-22**), the maximum temperature was higher in the order of the CETs located above the B21, B24, and B22 or B23 rod bundles.

Concerning the CETs at the peripheral region of UCP (**Fig. 4-23**), the maximum temperatures located above the B18 and B19 rod bundles were higher than those situated above other rod bundles. The maximum temperatures located above the B09 and B12 rod bundles were higher than those situated above the B10 and B14 rod bundles. Large decreases

appeared in the CETs located above the B11 and B15 rod bundles earlier than in those situated above other rod bundles.

Regarding the CETs at the outer region of UCP (**Fig. 4-24**), the maximum temperatures located above the B07 and B08 rod bundles were slightly higher than those situated above other rod bundles. The CETs located above the B03 and B04 rod bundles greatly dropped earlier than those situated above other rod bundles.

Figures 4-25 through 4-28 show the typical cladding surface temperatures of the simulated fuel rods at Positions 9 through 1. Positions 9, 8, 7, 6, 5, 4, 3, 2, and 1 are placed at 3.610 m, 3.048 m, 2.642 m, 2.236 m, 1.830 m, 1.242 m, 1.108 m, 0.612 m, and 0.050 m respectively above the core bottom (see p.222 in Ref. [5]). The representative cladding surface temperatures stand for the cladding surface temperatures of the rod bundles where the highest temperature emerges at each position. The arrangement of high-, mean-, and low-power rod bundles is presented in Ref. [5] (p.228). The cladding surface temperatures were affected by the axial core power profile (i.e., the 9-step chopped cosine) and the core liquid level behavior (**Figs. 4-18 and 4-19**). No cladding surface temperatures at Positions 2 and 1 rose. During the core uncover period the cladding surface temperatures at Positions 9, 8, 7, 6, 5, 4, and 3 began to increase at 14950 s, 14950 s, 14990 s, 15090 s, 15170 s, 15280 s, and 15400 s, respectively. The peak cladding temperature of 790 K was observed at Position 7 at 15550 s after the liquid level recovered in the SG secondary-side at 15500 s (**Fig. 4-8**). The cladding surface temperatures at Positions 9, 8, 6, 5, 4, and 3 reached 732 K at 15575 s, 781 K at 15585 s, 787 K at 15555 s, 771 K at 15580 s, 719 K at 15530 s, and 658 K at 15535 s, respectively. The cladding surface temperature at Position 9 initiated a large decrease at 15750 s. After around 15920 s the cladding surface temperatures at Positions 8 and 7 began to decrease, while those at Positions 6, 5, and 4 changed to rise. A great decline in the cladding surface temperature at Position 3 started at 16070 s. The cladding surface temperatures at Positions 6, 5, and 4 began to substantially drop at 16290 s, 16310 s, and 16285 s, respectively. This resulted from a significant increase in the core liquid level following the activation of the ACC system at 16210 s (**Figs. 4-12 and 4-19**). The entire core was quenched by 16320 s due to the core liquid level recovery because of coolant injection from the ACC system into both cold legs.

Figures 4-29, 4-30, 4-31, 4-32, 4-33, 4-34, and 4-35 show the distributions of the cladding surface temperatures of the simulated fuel rods at Positions 9, 8, 7, 6, 5, 4, and 3, respectively. At Position 9 (**Fig. 4-29**), the cladding surface temperature rises of the B17 and B22 rod bundles were earlier than that of the B08 rod bundle. The maximum cladding surface temperature was higher in the order of the B22, B17, and B08 rod bundles. The quenching of the cladding surface was faster in the order of the B08, B17, and B22 rod bundles.

At Position 8 (**Fig. 4-30**), the cladding surface temperature increases of the B10 and B13 rod bundles were earlier than that of the B03 rod bundle. The maximum cladding surface temperature was higher in the order of the B13, B10, and B03 rod bundles. The cladding surface was quenched faster in the order of the B03, B10, and B13 rod bundles.

At Position 7 (**Fig. 4-31**), the cladding surface temperature rises of the B10, B13, B17, and B22 rod bundles were earlier than those of the B03 and B08 rod bundles. The maximum cladding surface temperature of the B13 rod bundle was higher than those of other rod bundles. The maximum cladding surface temperature of the B08 rod bundle was nearly equal to those of the B17 and B22 rod bundles. The maximum cladding surface temperature was higher in the order of the B08, B10, and B03 rod bundles. The quenching of the cladding surface was faster in the order of the B03, B08, B10, B22, B13, and B17 rod bundles.

At Position 6 (**Fig. 4-32**), the cladding surface temperatures of the B03, B10, and B13 rod bundles rose almost simultaneously. The maximum cladding surface temperature was higher in the order of the B13, B10, and B03 rod bundles. The cladding surface was quenched faster in the order of the B03, B10, and B13 rod bundles.

At Position 5 (**Fig. 4-33**), the cladding surface temperatures of the B08, B17, and B22 rod bundles rose at almost the same time. The maximum cladding surface temperature was higher in the order of the B17, B08, and B22 rod bundles. The quenching of the cladding surface was faster in the order of the B08, B22, and B17 rod bundles.

At Position 4 (**Fig. 4-34**), the cladding surface temperatures of the B03, B10, and B13 rod bundles rose almost simultaneously. The maximum cladding surface temperature was higher in the order of the B13, B10, and B03 rod bundles. The cladding surface was quenched faster in the order of the B03, B10, and B13 rod bundles.

At Position 3 (**Fig. 4-35**), the cladding surface temperatures of the B08, B17, and B22 rod bundles rose at almost the same time. No marked difference laid in the maximum cladding surface temperature among the B08, B17, and B22 rod bundles. The quenching of the cladding surface was faster in the order of the B08, B22, and B17 rod bundles.

Coolant behaviors in pressure vessel

Figure 4-36 shows the downcomer collapsed liquid level. The liquid level appeared in the downcomer at 1080 s. A considerable drop initiated in the downcomer liquid level at 14350 s. The liquid level recovered in the downcomer at 16250 s with the coolant injection from the ACC system into the cold legs (**Fig. 4-12**). The downcomer liquid level was held at around 5.5-5.7 m after the termination of the ACC coolant injection at 17370 s.

Figure 4-37 shows the upper-head collapsed liquid level. An abrupt depression started in

the upper-head liquid level at 1270 s. The upper-head liquid level was maintained at around 0.05-0.10 m after 1850 s.

4.3.2 Thermal-hydraulic Responses in Primary Loops

Figures 4-38 and 4-39 show the liquid levels and fluid temperatures in the hot legs, respectively. The hot leg liquid level is estimated from the fluid densities measured by use of a three-beam gamma-ray densitometer. The hot leg fluid became saturated at 880 s almost concurrently with the liquid level formation in the hot leg. The liquid level in the hot leg with an inner-diameter of 0.207 m was kept at around 0.155-0.175 m in both loops at around 2000-14200 s. The hot leg liquid level became lost at 14620 s after an abrupt decrease initiated in the upper plenum liquid level at 14450 s (**Fig. 4-17**). The liquid level recovered in the hot leg by coolant from the PZR (**Fig. 4-13**). The hot leg liquid level rose with the ACC coolant injection into the cold leg (**Fig. 4-12**). The hot leg liquid level was held at around 0.100-0.115 m after the termination of the ACC coolant injection at 17370 s. The hot leg fluid temperature indicated superheating during the two time periods of around 15220-15700 s and around 16100-16500 s. The hot leg fluid temperature showed subcooling after around 17200 s.

Figures 4-40 and 4-41 show the liquid levels and fluid temperatures in the cold legs, respectively. The cold leg liquid level is evaluated from the fluid densities measured by means of a three-beam gamma-ray densitometer. The cold legs were filled with subcooled water until the primary pressure dropped to around 10 MPa (**Fig. 4-14**). The liquid levels formed in the cold legs at around 1500 s. When the liquid level in the cold leg with an inner-diameter of 0.207 m depressed to around 0.17 m, the cold leg fluid became saturated. The cold leg liquid level once became close to zero just before the third AM action start. When the cold leg liquid level rose up to around 0.15 m resulting from the ACC coolant injection (**Fig. 4-12**), the cold leg fluid temperature indicated subcooling. The cold leg fluid temperature increased with a reduction in the cold leg liquid level after the termination of the ACC coolant injection. The cold leg liquid level became close to zero afterwards.

Figures 4-42 and 4-43 show the collapsed liquid levels in the downflow-side and upflow-side of the crossover legs, respectively. The crossover leg downflow-side liquid level started to drop at 12000 s, and then turned to rise at 14300 s. The crossover leg upflow-side liquid level began a decline at 15580 s. During the ACC coolant injection period (**Fig. 4-12**) the liquid levels in the downflow-side and upflow-side of the crossover legs decreased and increased, respectively.

4.3.3 Thermal-hydraulic Responses of Steam Generators

Figures 4-44 through 4-47 show the collapsed liquid levels in the instrumented SG U-tubes. The instrumented SG U-tubes designated as Tubes 1 and 6 are short tubes (Type 1; see p.267

in Ref. [5]), Tubes 2 and 5 are medium tubes (Type 5), and Tubes 3 and 4 are long tubes (Type 9). The liquid level in the upflow-side balanced that in the downflow-side for each SG U-tube. The trend of the liquid level change was comparable for the two same-length SG U-tubes consisting of short, medium, and long tubes. However, the liquid level behaviors in the SG U-tubes were asymmetrical between two loops. Considerable drain of the water column initiated the earliest in Tube 6 and the latest in Tube 2 among the U-tubes of both SGs. The liquid level drop in the downflow-side and upflow-side of the SG U-tubes continued down to the crossover leg downflow-side (**Fig. 4-42**) and the SG inlet plenum (to be plotted in **Fig. 4-52**), respectively. Resultantly, the SG U-tubes became voided. The liquid levels recovered in the downflow-side and upflow-side of the SG U-tubes at around 17350 s and around 17000 s respectively with the ACC coolant injection into the cold legs (**Fig. 4-12**). Non-uniform flow behaviors were found in the SG U-tubes with nitrogen gas ingress. The water column drained faster in Tubes 1 and 6 and slower in Tubes 2 and 5 among the U-tubes of both SGs. At 28000 s the liquid level in each U-tube of SG in loop with PZR remained at a certain liquid level while the U-tubes of SG in loop without PZR were emptied of liquid.

To investigate the accumulating status of nitrogen gas in the SG U-tube, nitrogen gas mole fraction M in the steam-gas mixture is expressed by

$$M = \frac{P - P_s}{P} \quad (1)$$

where P is the total pressure of the steam-gas mixture that is represented by the PZR pressure (**Fig. 4-14**). P_s is the steam pressure that is equivalent to the steam saturation pressure based on the SG U-tube fluid temperature by assuming 100% relative humidity of saturated steam in the steam-gas mixture. The fluid temperatures in the downflow-side of the SG U-tubes at Position 7 (= at 5.941 m above the SG U-tube bottom) were chosen as the SG U-tube fluid temperatures for evaluating the nitrogen gas mole fraction. This selection took account of the SG U-tube liquid level behaviors (**Figs. 4-44 through 4-47**). **Figures 4-48 and 4-49** show the fluid temperatures at Position 7 in the downflow-side of the SG U-tubes in loops with and without PZR respectively from 18000 s to 20000 s. Here, the fluid temperatures of Tube 1 (one of two short tubes) in loop with PZR and Tube 2 (one of two medium tubes) in loop without PZR were unavailable on account of the bad trends. The tendency of the fluid temperature variation was similar for the identical-length SG U-tubes until around 18400 s. The SG U-tube fluid temperature became the same afterwards. The SG U-tube fluid temperature was lower in loop with PZR than in loop without PZR. **Figures 4-50 and 4-51** show the estimated nitrogen gas mole fractions of the SG U-tubes in loops with and without PZR, respectively. The nitrogen gas mole fractions of the SG U-tubes exceeded zero since around 18200 s. At around 18400 s the nitrogen gas mole fractions of the SG U-tubes in loops with and without PZR were evaluated to be approximately 0.40 and 0.35, respectively. Most of the

nitrogen gas mole fractions of the SG U-tubes gradually increased thereafter. The nitrogen gas mole fraction of the SG U-tube in loop with PZR was generally greater than that in loop without PZR. The reason is that the steam pressure P_s was lower in loop with PZR than in loop without PZR, relying on the SG U-tube fluid temperature. The cold leg in loop without PZR has the break, whereas the break flow area accorded with 0.1% of the 1/48-scaled cross-sectional area of the reference PWR cold leg is very small. However, this may affect the difference in the nitrogen gas mole fractions of the SG U-tubes between the two loops.

Figure 4-52 shows the SG inlet plenum collapsed liquid level. A substantial depression initiated in the SG inlet plenum liquid level at 13700 s. The SG inlet plena became empty of liquid at 14230 s. The liquid levels recovered in the SG inlet plena at around 16560 s with the ACC coolant injection into the cold legs (**Fig. 4-12**).

Figures 4-53 and 4-54 show the SG secondary-side fluid temperatures in loops with and without PZR, respectively. Positions 1, 3, 5, 7, and 9 are placed at 0.811 m, 2.101 m, 3.381 m, 5.941 m, and 8.501 m respectively above the SG U-tube bottom. Depending on the SG secondary-side liquid level (**Fig. 4-8**) the SG secondary-side fluid temperatures at Positions 1, 3, 5, 7, and 9 showed superheating after 8000 s, 6500 s, 5100 s, 4300 s, and 3000 s, respectively. The SG secondary-side fluid temperatures at Positions 1, 3, 5, 7, and 9 were mostly maintained saturated after 15500 s, 17000 s, 17500 s, 18300 s, and 19120 s, respectively.

Table 4-1 Initial steady state conditions

Items	Tag Name (Loops with / without PZR)	Specified (Loops with / without PZR)	Measured *1 (Loops with / without PZR)
Pressure vessel			
Core power (MW)	WE270A-T	10.0±0.07	10.10
Downcomer-to-upper head bypass (%)	None	0.3	Not measured
Primary loop			
Hot leg fluid temperature (K)	TE020C-HLA / TE160C-HLB	598.1±2.75	597.7 / 597.7
Cold leg fluid temperature (K)	TE070C-CLA / TE210C-CLB	562.4±2.75	563.5 / 563.5
Mass flow rate (kg/s / loop)	FE020A-LSA / FE160A-LSB	24.3±1.25	24.83 / 24.75
Downcomer-to-hot leg bypass (kg/s)	FE010-HLA / FE150-HLB	0.049±0.01	0.050 / 0.047
Pressurizer (PZR)			
Pressure (MPa)	PE300A-PR	15.5±0.108	15.62
Liquid level (m)	LE280-PR	7.2±0.25	7.44
Steam generator			
Secondary-side pressure (MPa)	PE430-SGA / PE450-SGB	7.3±0.054	7.31 / 7.35
Secondary-side liquid level (m)	LE430-SGA / LE450-SGB	10.3±0.38	10.26 / 10.24
Steam flow rate (kg/s)	FE440-SGA / FE480-SGB	2.74±0.10	2.63 / 2.67
Main feedwater flow rate (kg/s)	FE430-SGA / FE470-SGB	2.74±0.05	2.70 / 2.69
Main feedwater temperature (K)	TE430-SGA / TE470-SGB	495.2±2.63	497.0 / 496.1
Temperature of water injection into secondary-side through feedwater line (K)	TE880-RWST	310±2.37	311.0
Accumulator system			
Pressure (MPa)	PE650-ACC / PE660-ACH	4.51±0.054	4.57 / 4.55
Temperature (K)	TE660-ACC / TE700-ACH	320±2.3 / 2.4	320.9 / 321.5
Water level above tank bottom (m) *2	LE650-ACC / LE660-ACH	6.8±0.12/0.15	6.81 / 6.81

*1 Averaged for 60 s (-60 to 0 s)

*2 Distance from standpipe top to tank bottom is 5.22 m.

Table 4-2 Chronology of major events until break valve closure

Time (s)	Event
0	Break valve open, scram signal, start of primary coolant pumps rotation speed increase (to 1470 rpm in 4 s)
1	Closure of SG main steam stop valve
2	Termination of SG main feedwater
3	Manual closure of SG main steam isolation valves
19	Initiation of coastdown of primary coolant pumps
20	Initiation of core power decay
190-8120	Cycle opening of safety valves in both SGs
269	Stop of primary coolant pumps
529	PZR backup heater power off
760	PZR liquid level became lost.
8130	Secondary-side of both SGs became empty of liquid.
9250	Initiation of PZR liquid level recovery
13680-15030	Cycle opening of safety valve of PZR
14950	Initiation of increases in cladding surface temperatures at Positions 9 and 8 by core boil-off
15020	Initiation of SG secondary-side depressurization by fully opening safety valves in both SGs as first AM action
15040	Initiation of primary depressurization by completely opening safety valve of PZR as second AM action
15150	Initiation of increase in core exit temperature at center of upper core plate
15360	Initiation of water injection into secondary-side of both SGs through feedwater lines employing AFW pumps as third AM action
15500	Initiation of SG secondary-side liquid level recovery
15515	Peak core exit temperature of 735 K was seen at center of upper core plate.
15550	Peak cladding temperature of 790 K was observed at Position 7.
16210	Initiation of ACC system in both loops
16320	Whole core quench
17020	PZR liquid level became lost again.
17370	Termination of ACC system in both loops
18200	Initiation of degradation in primary depressurization due to nitrogen gas accumulation in SG U-tubes
28818	Core power off
28833	Break valve closure

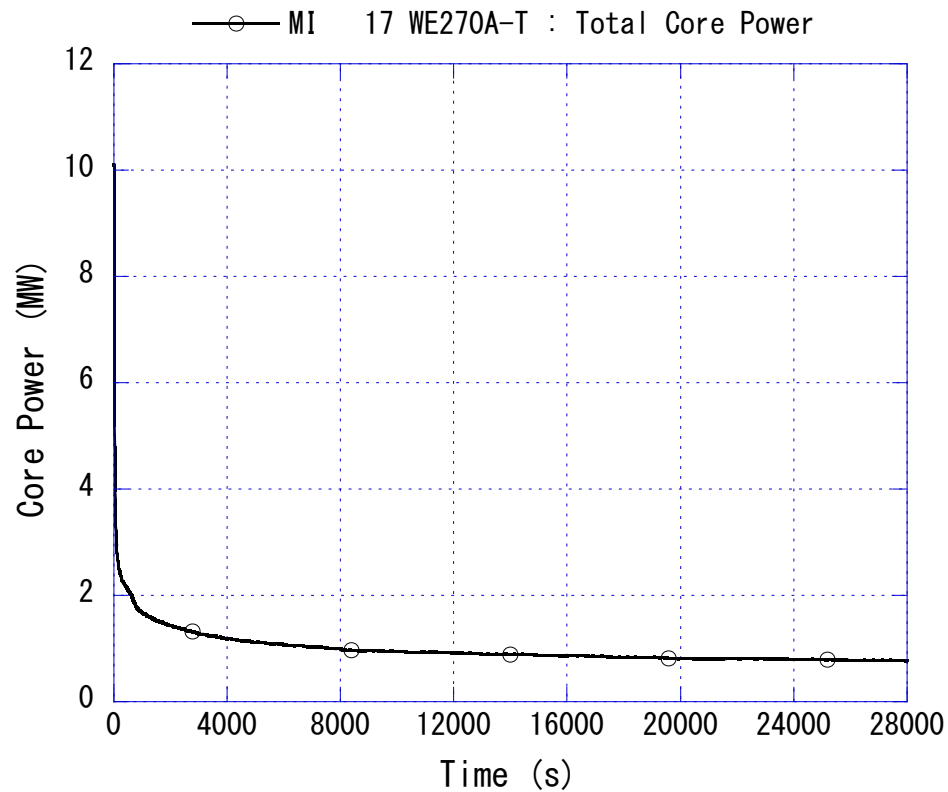


Fig. 4-1 Core power

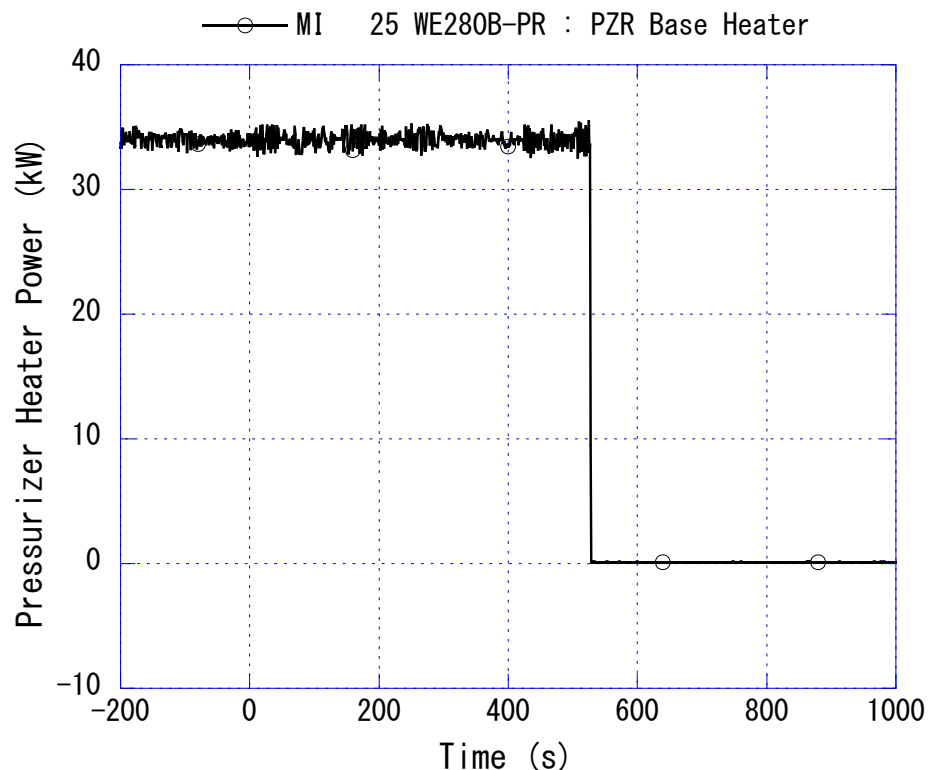


Fig. 4-2 Pressurizer heater power

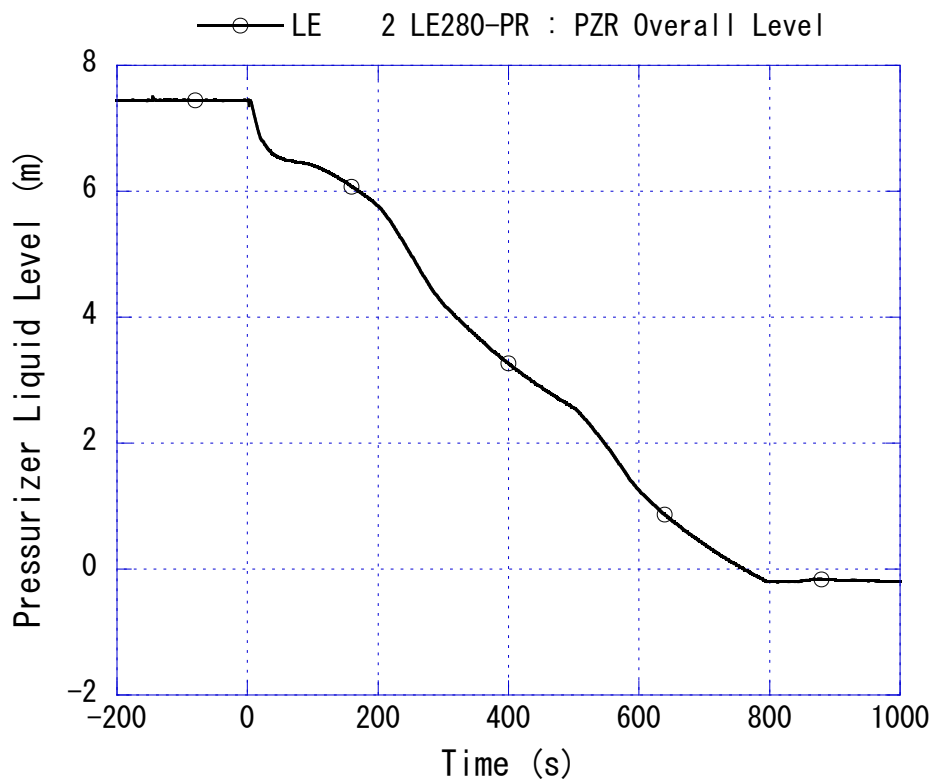


Fig. 4-3 Pressurizer liquid level (-200 to 1000 s)

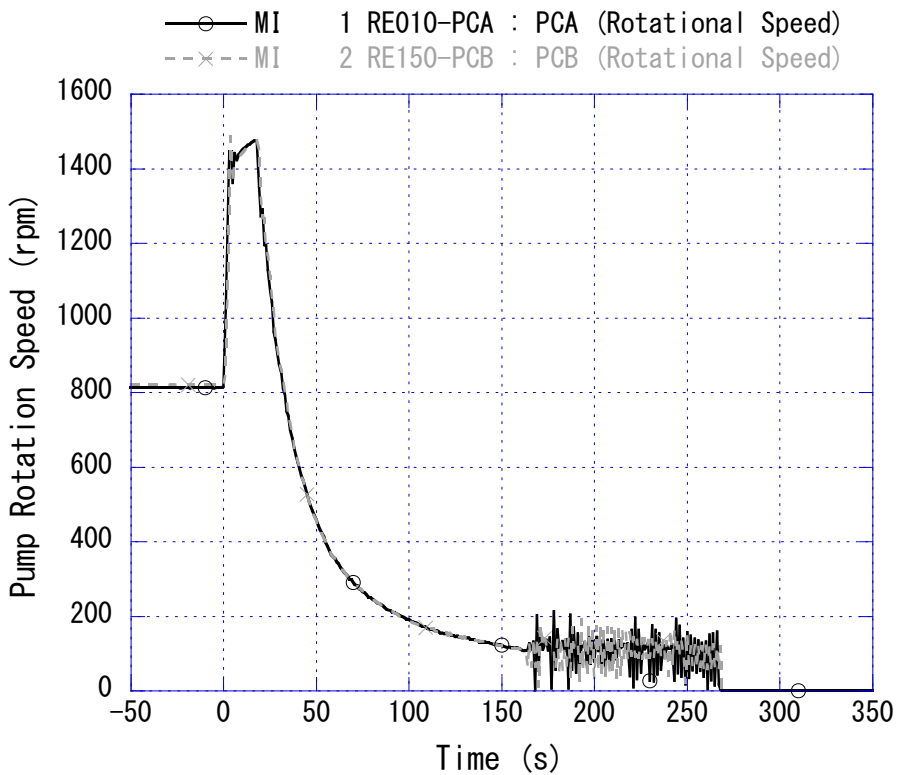


Fig. 4-4 Primary coolant pump rotation speed

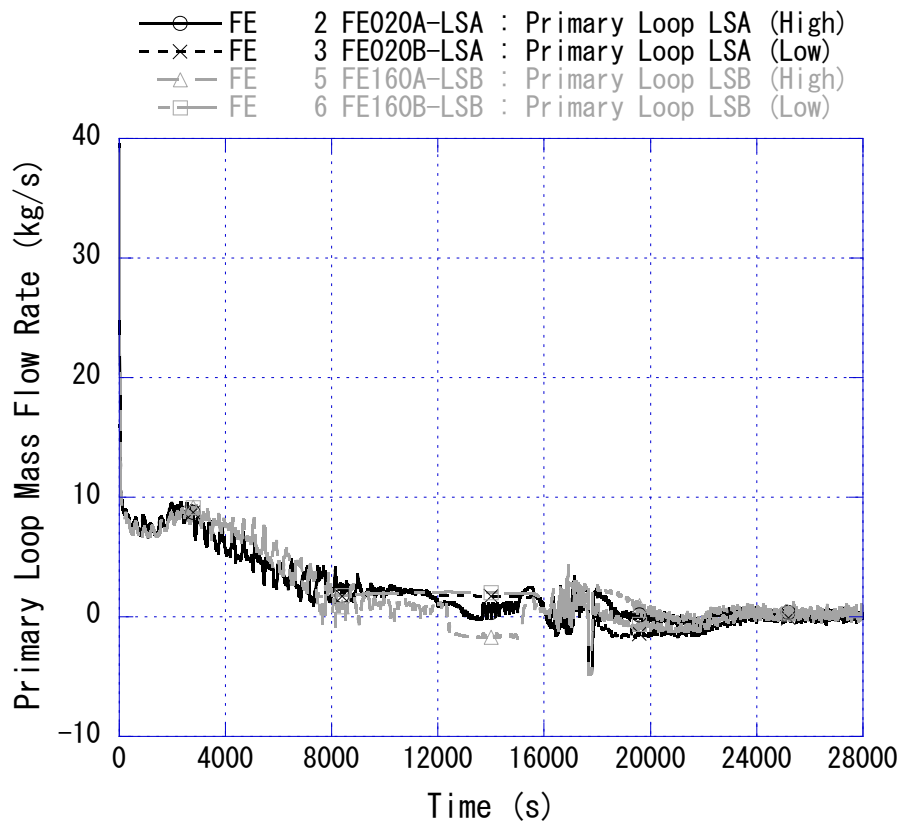


Fig. 4-5 Primary loop mass flow rate

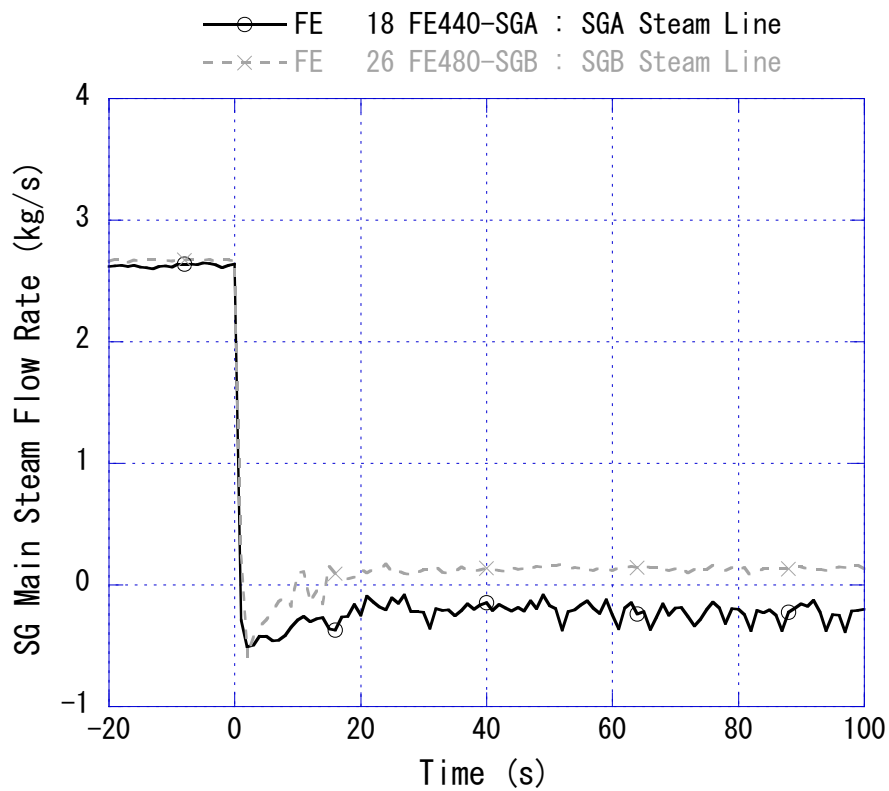


Fig. 4-6 SG main steam flow rate

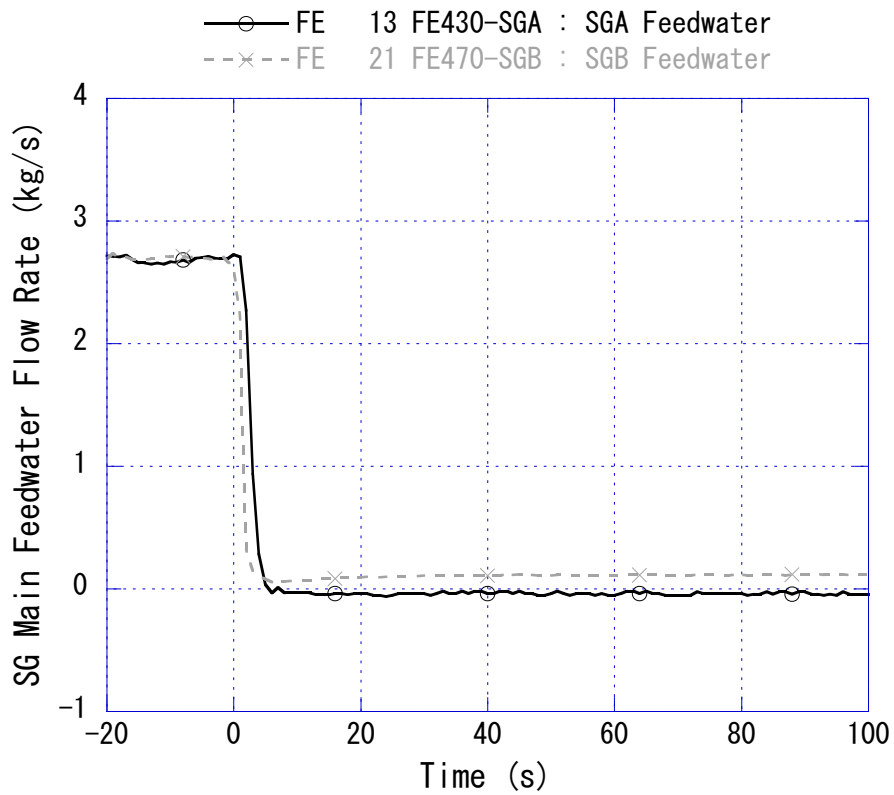


Fig. 4-7 SG main feedwater flow rate

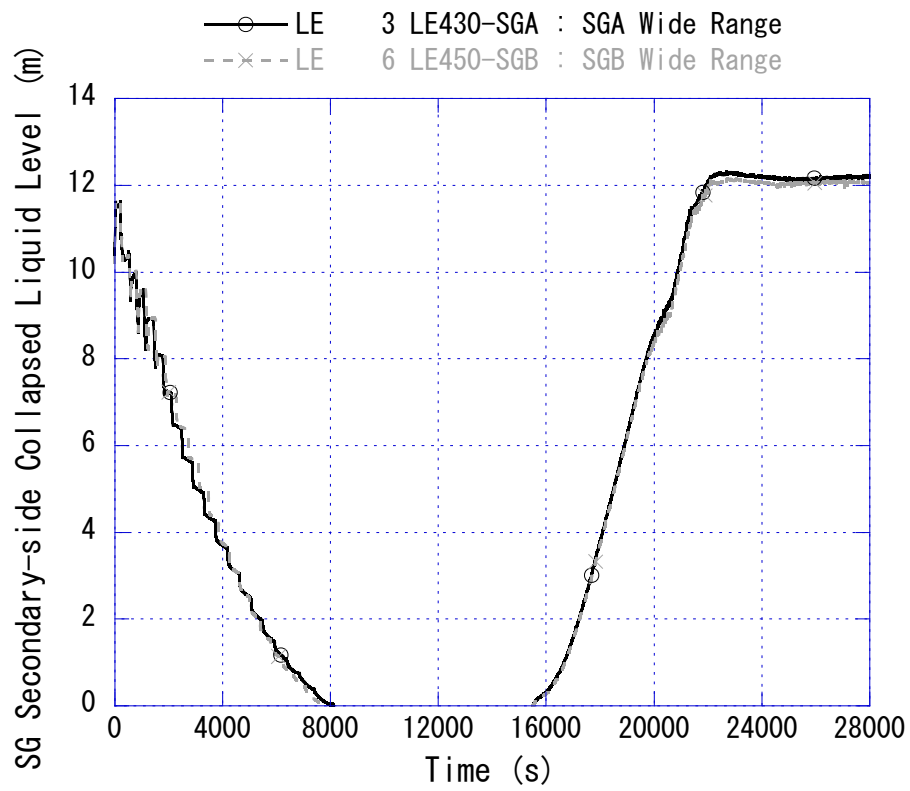


Fig. 4-8 SG secondary-side collapsed liquid level

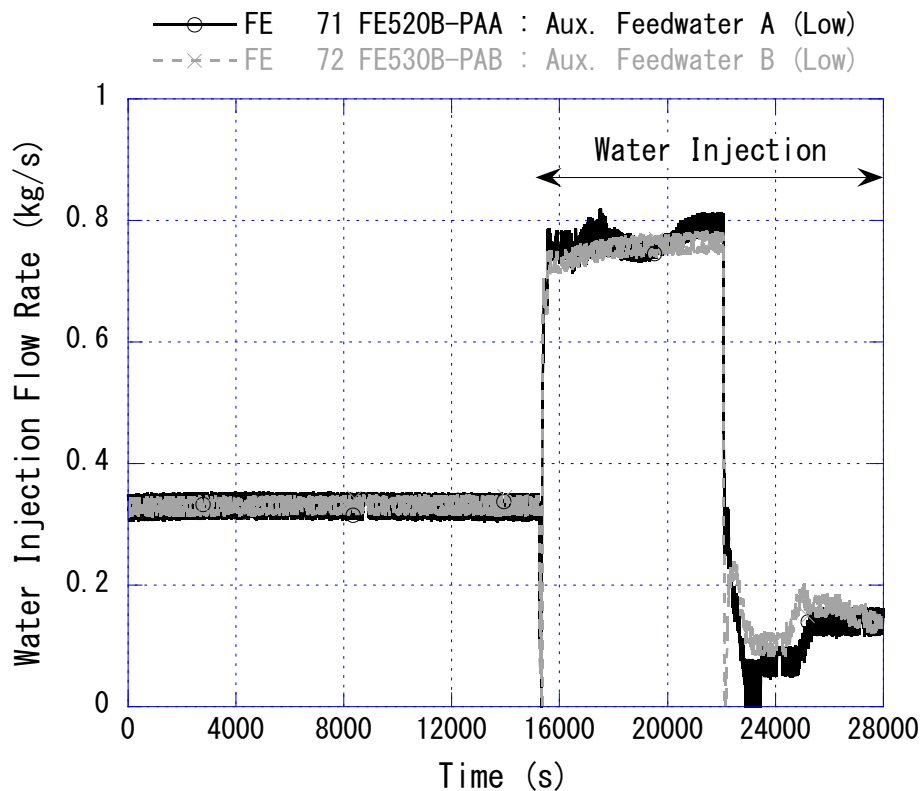


Fig. 4-9 Water injection flow rate into SG secondary-side via AFW pump

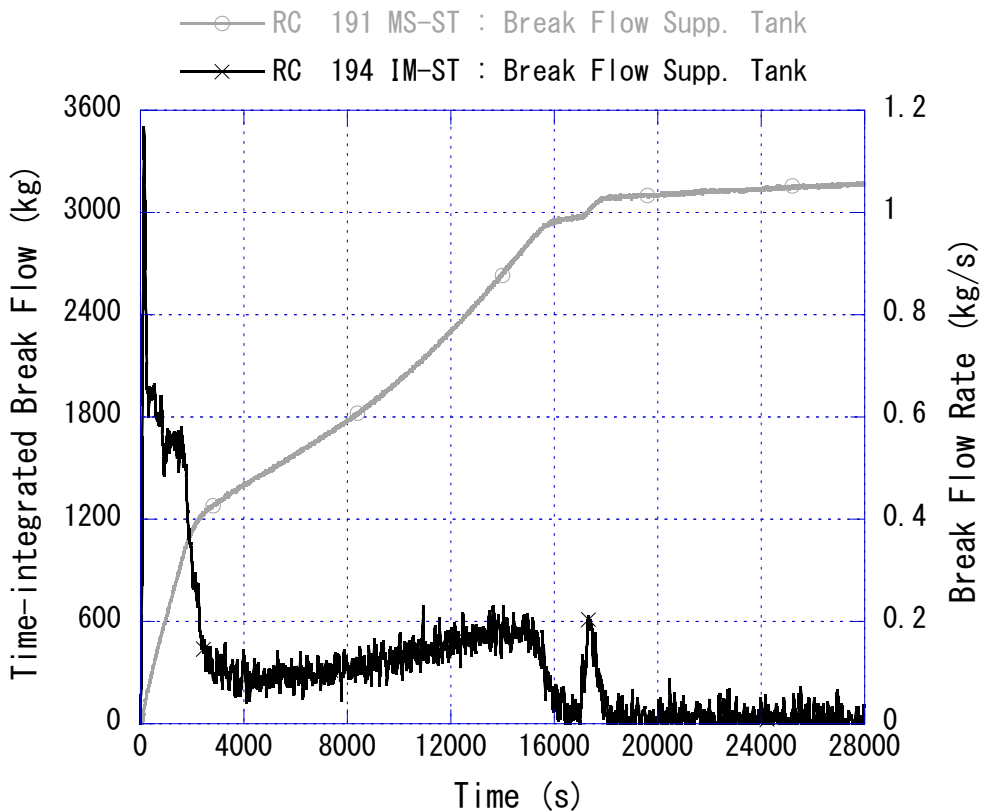


Fig. 4-10 Time-integrated break flow and break flow rate

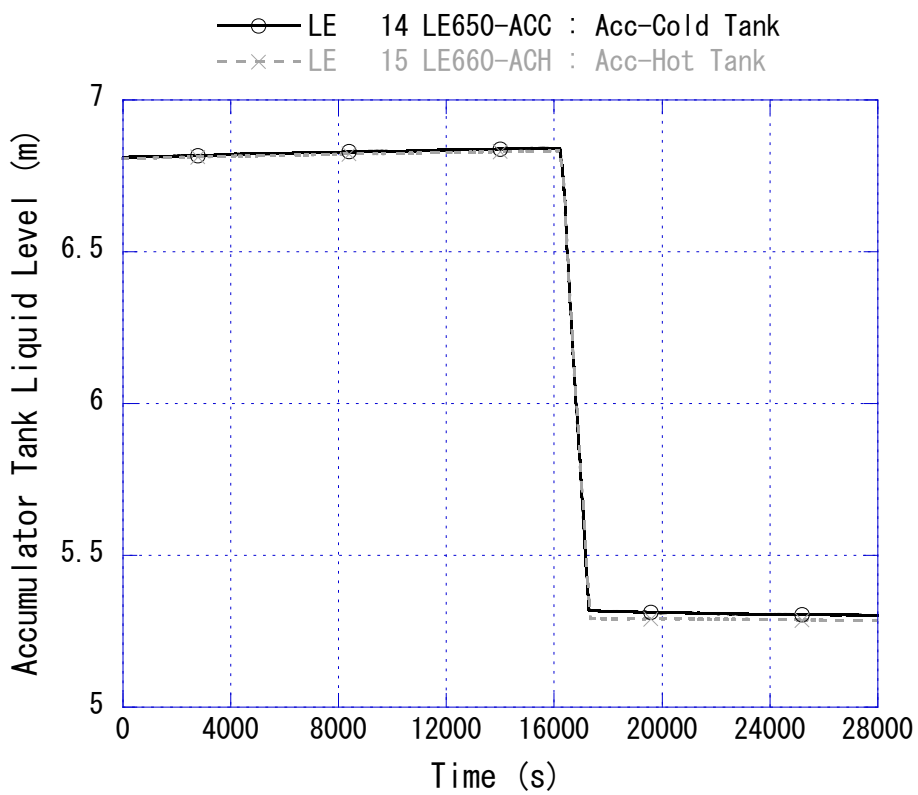


Fig. 4-11 Liquid level in accumulator tank

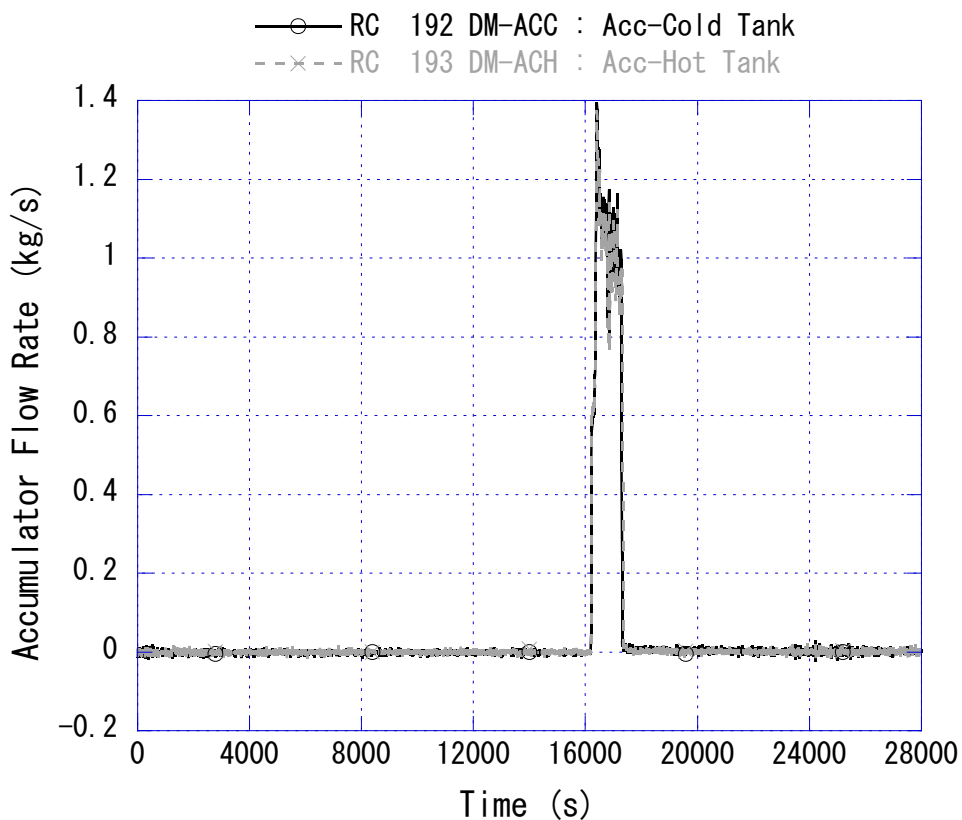


Fig. 4-12 Coolant injection flow rate from accumulator tank

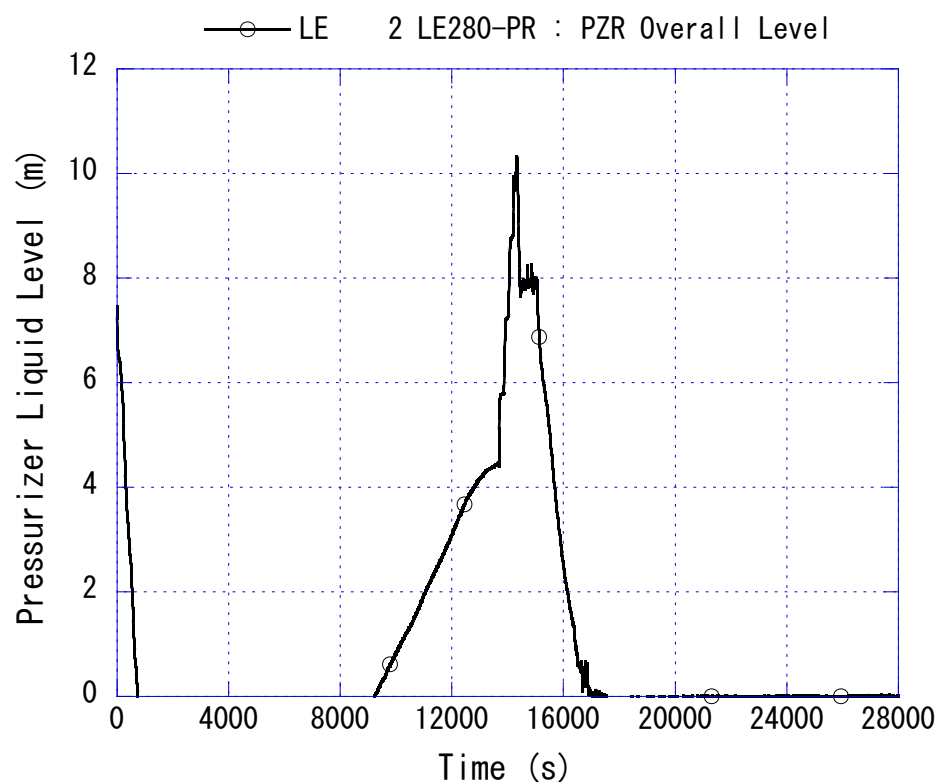


Fig. 4-13 Pressurizer liquid level (0 to 28000 s)

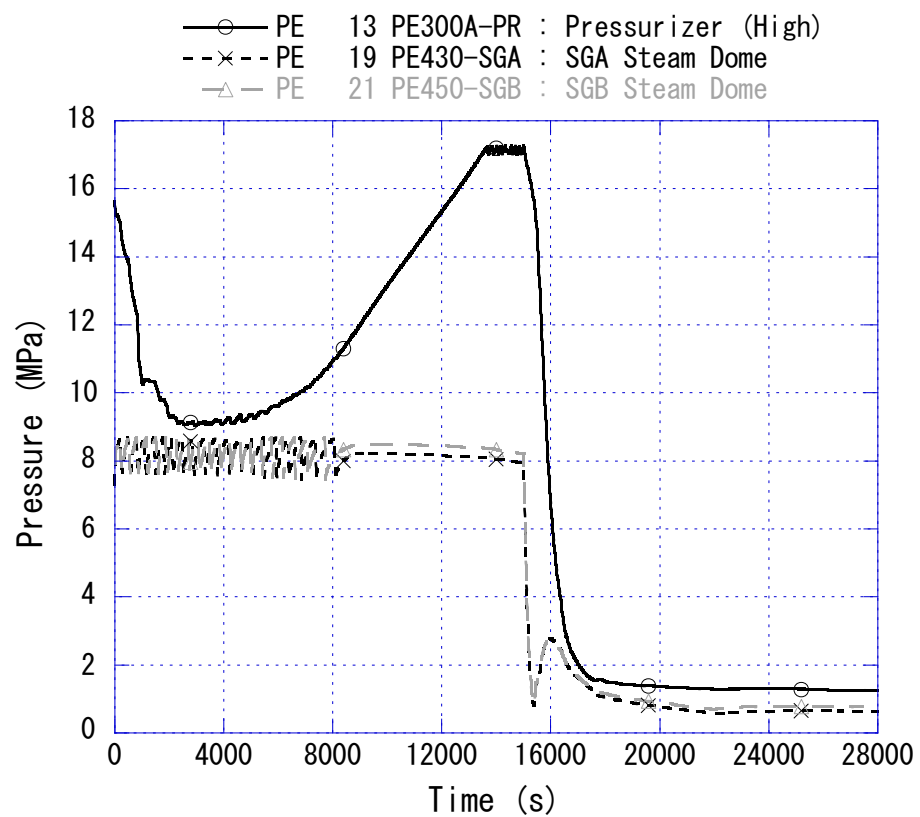


Fig. 4-14 Primary and secondary pressures (0 to 28000 s)

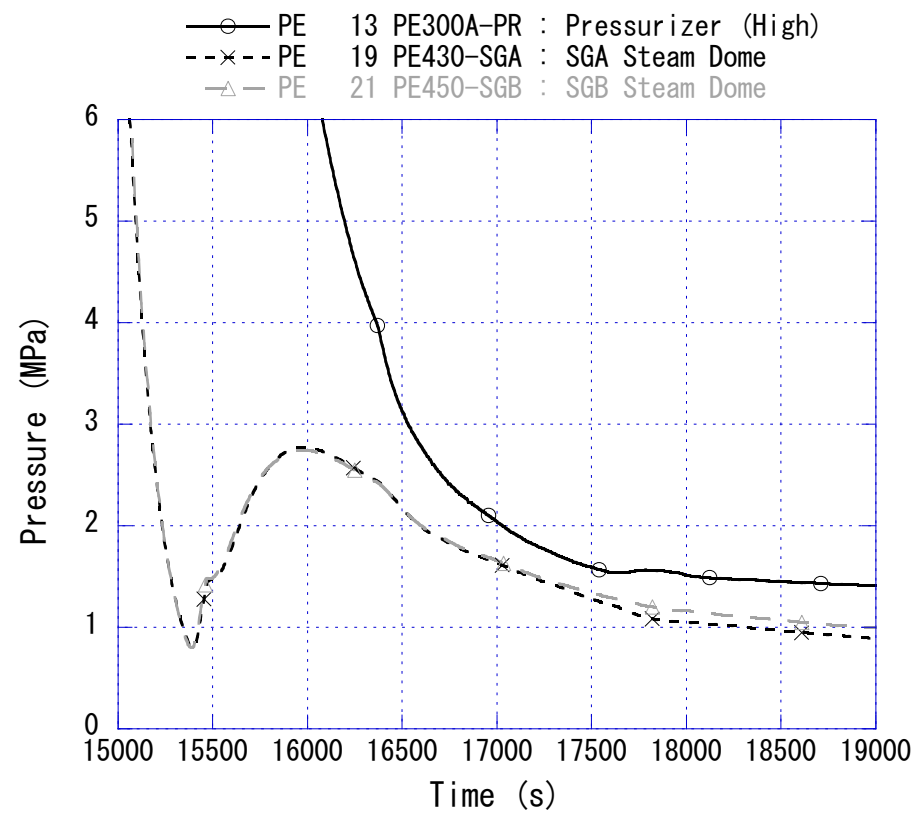


Fig. 4-15 Primary and secondary pressures (15000 to 19000 s)

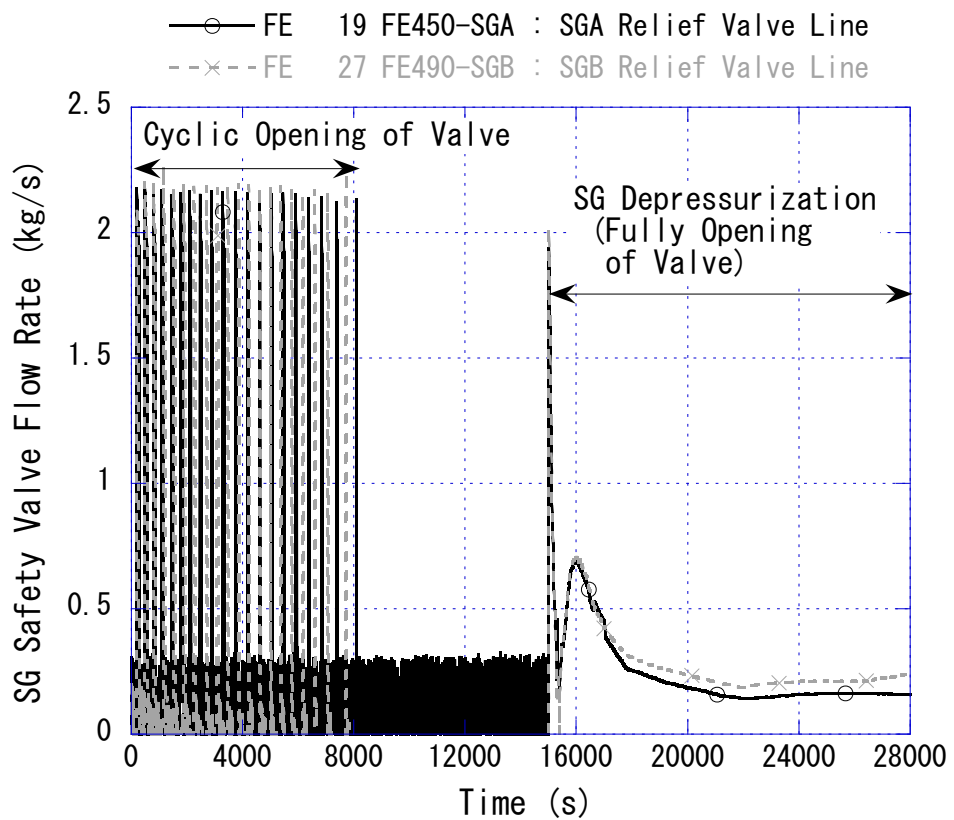


Fig. 4-16 SG safety valve flow rate

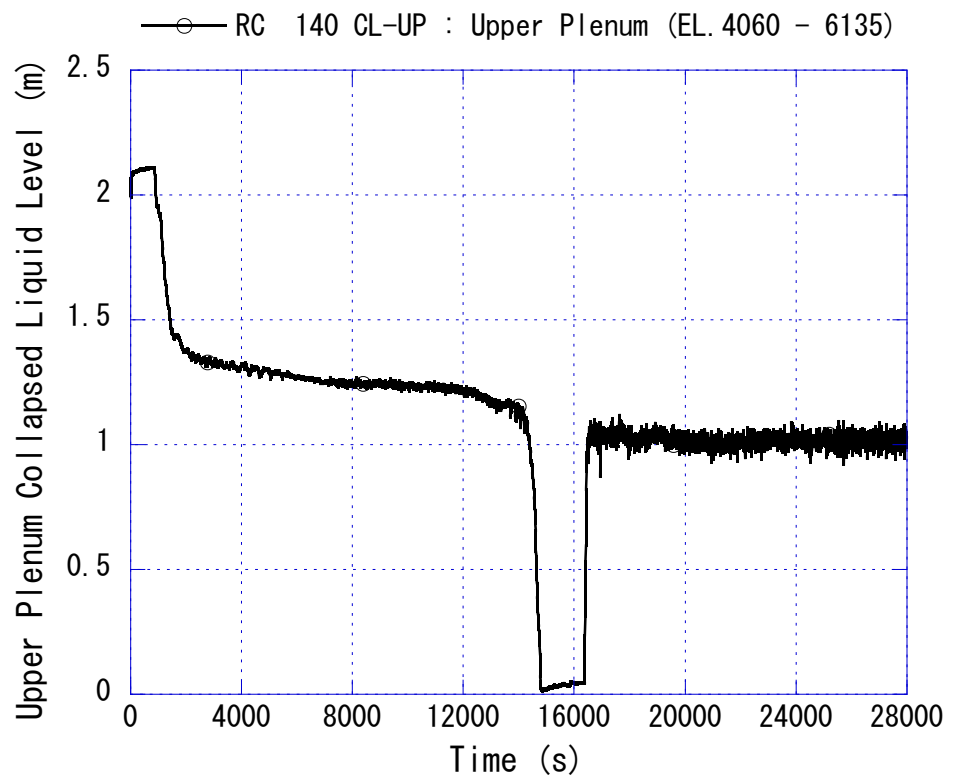


Fig. 4-17 Upper plenum collapsed liquid level

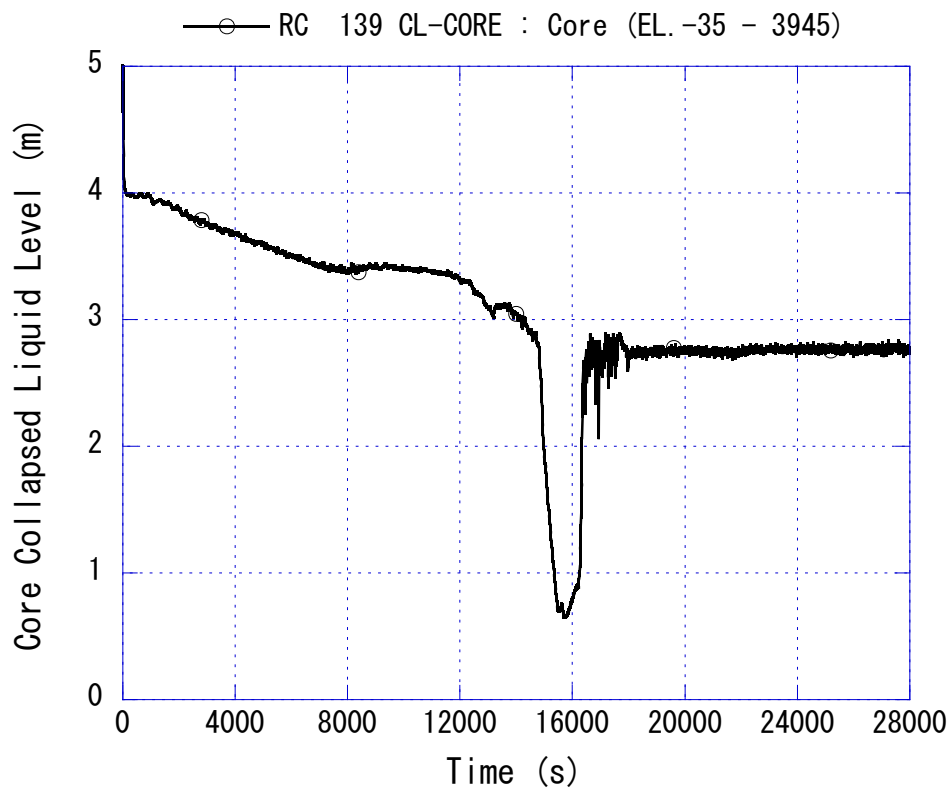


Fig. 4-18 Core collapsed liquid level (0 to 28000 s)

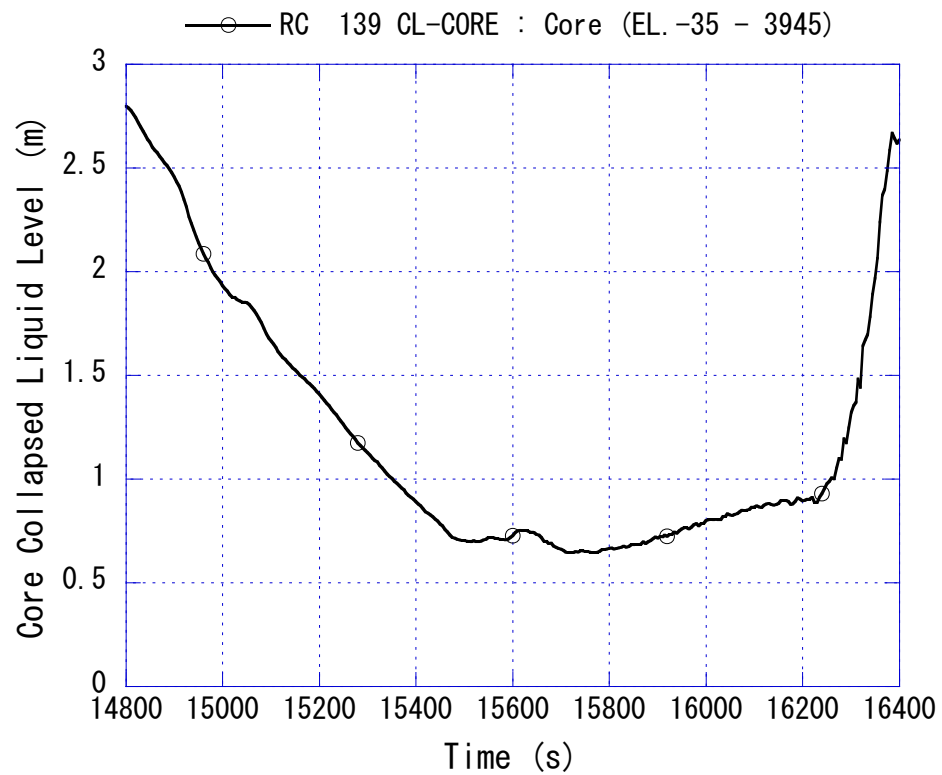


Fig. 4-19 Core collapsed liquid level (14800 to 16400 s)

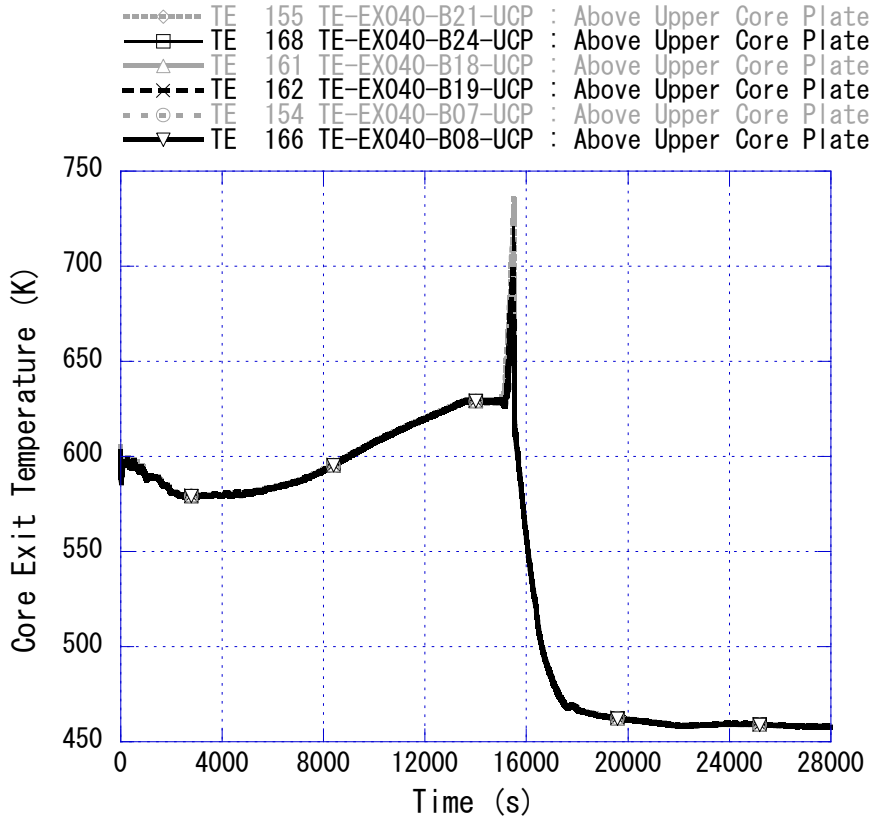


Fig. 4-20 Typical core exit temperatures (0 to 28000 s)

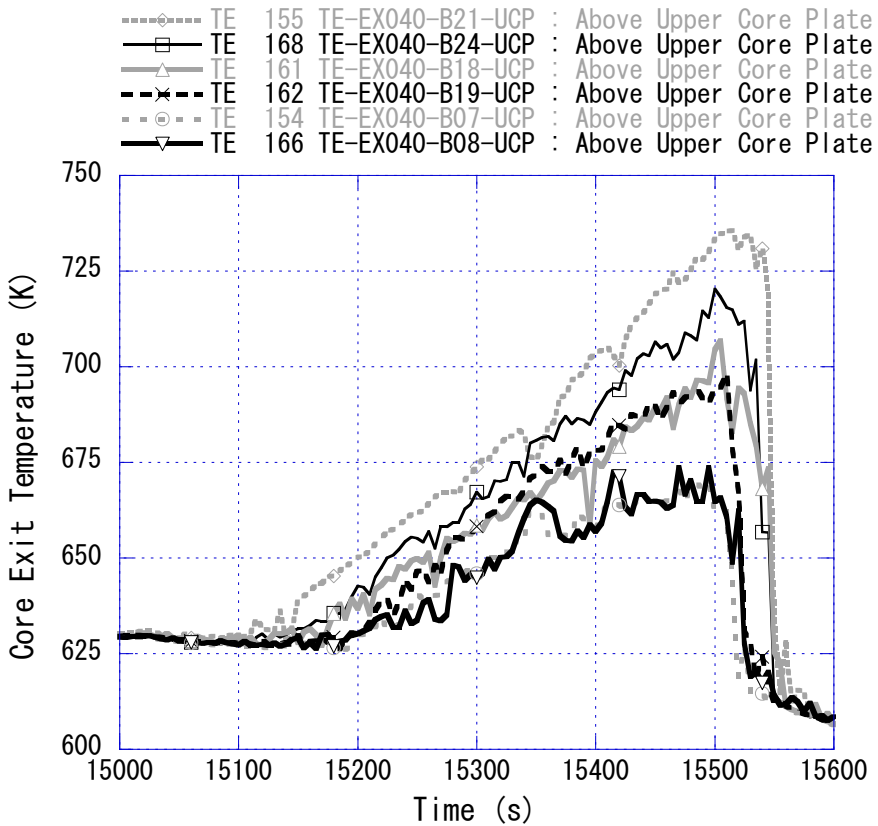


Fig. 4-21 Typical core exit temperatures (15000 to 15600 s)

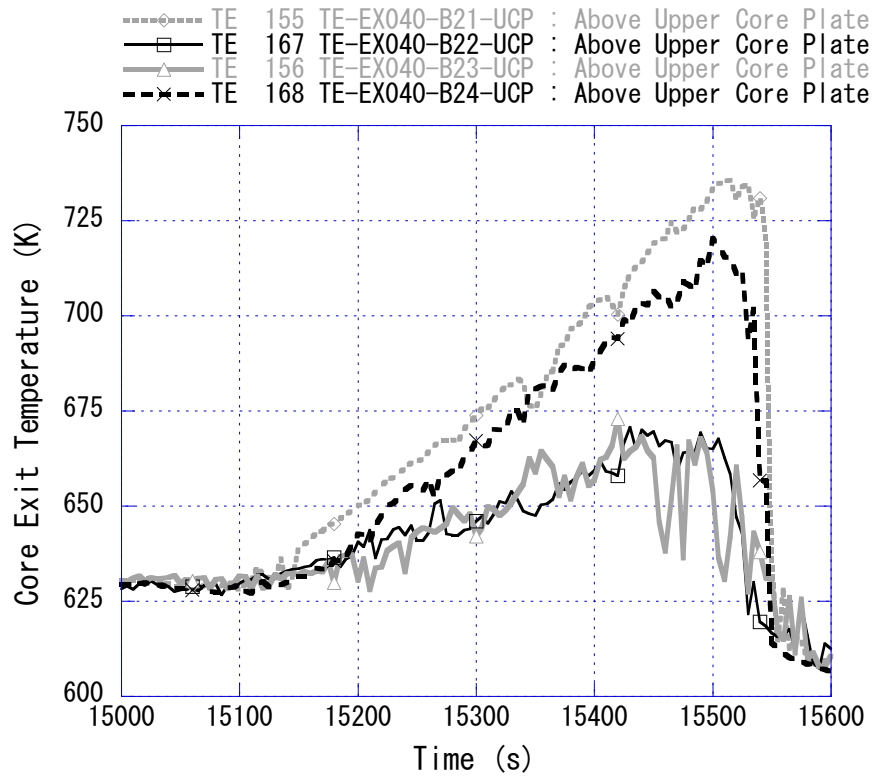


Fig. 4-22 Core exit temperatures at center of UCP (15000 to 15600 s)

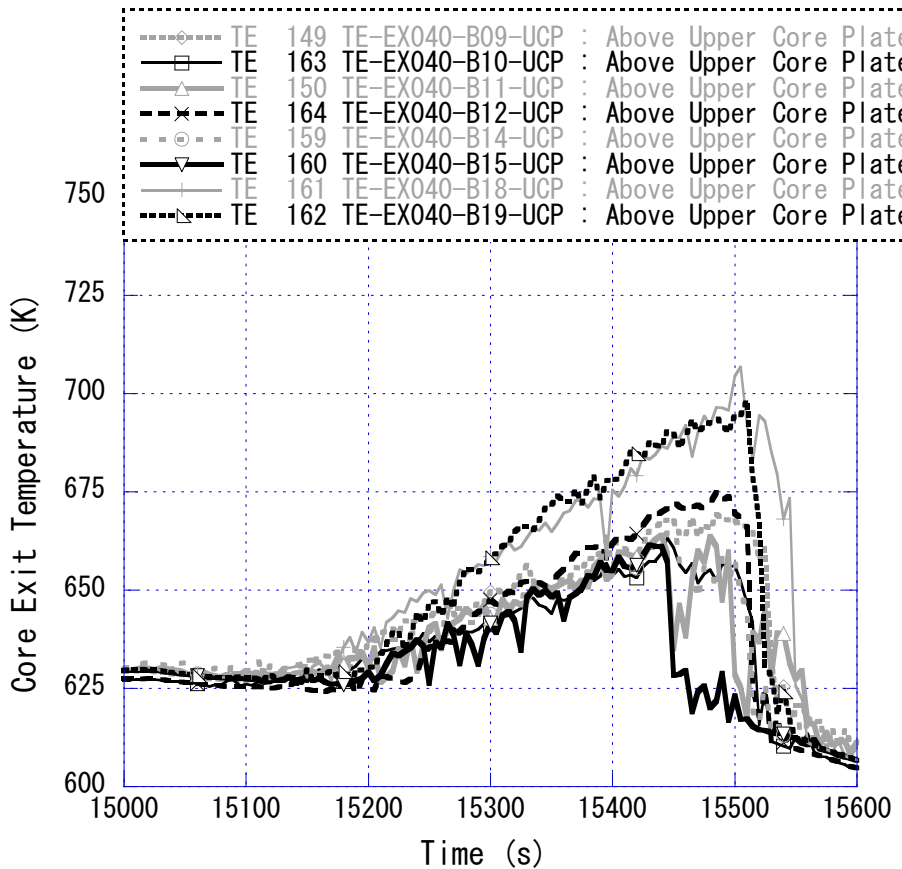


Fig. 4-23 Core exit temperatures at peripheral region of UCP (15000 to 15600 s)

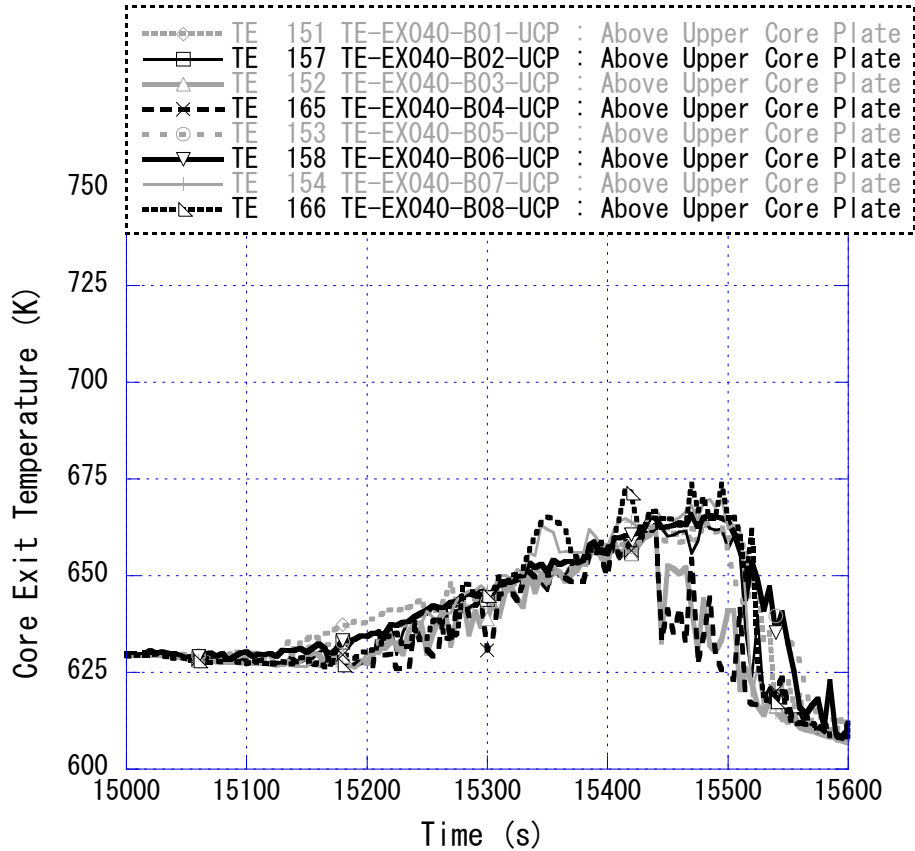


Fig. 4-24 Core exit temperatures at outer region of UCP (15000 to 15600 s)

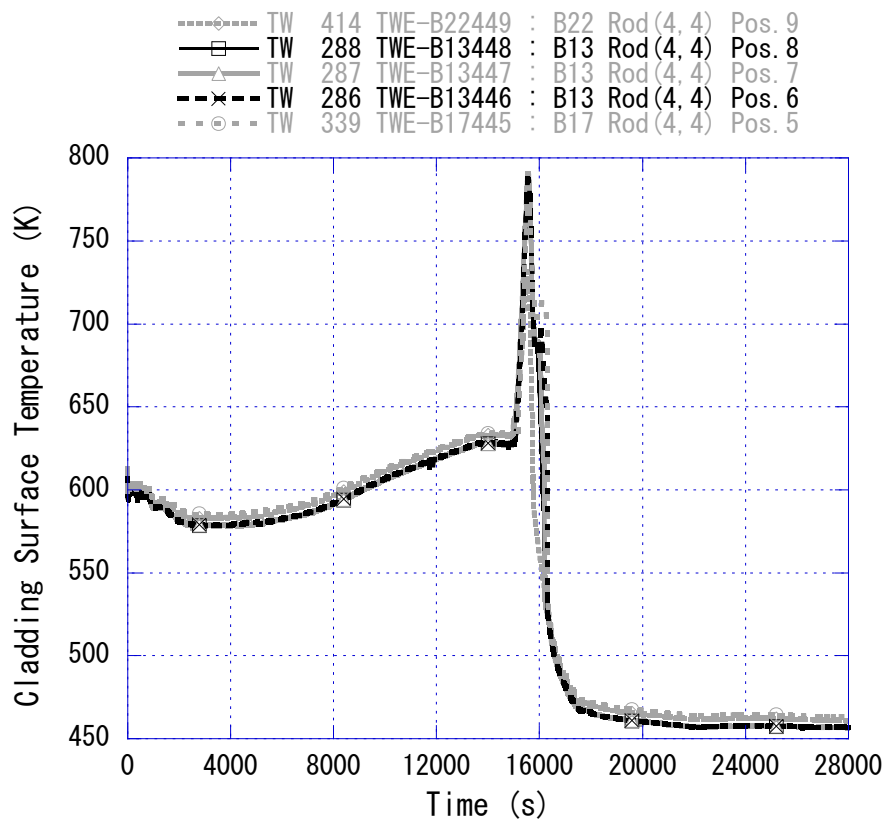


Fig. 4-25 Typical cladding surface temperatures at Positions 9-5 (0 to 28000 s)

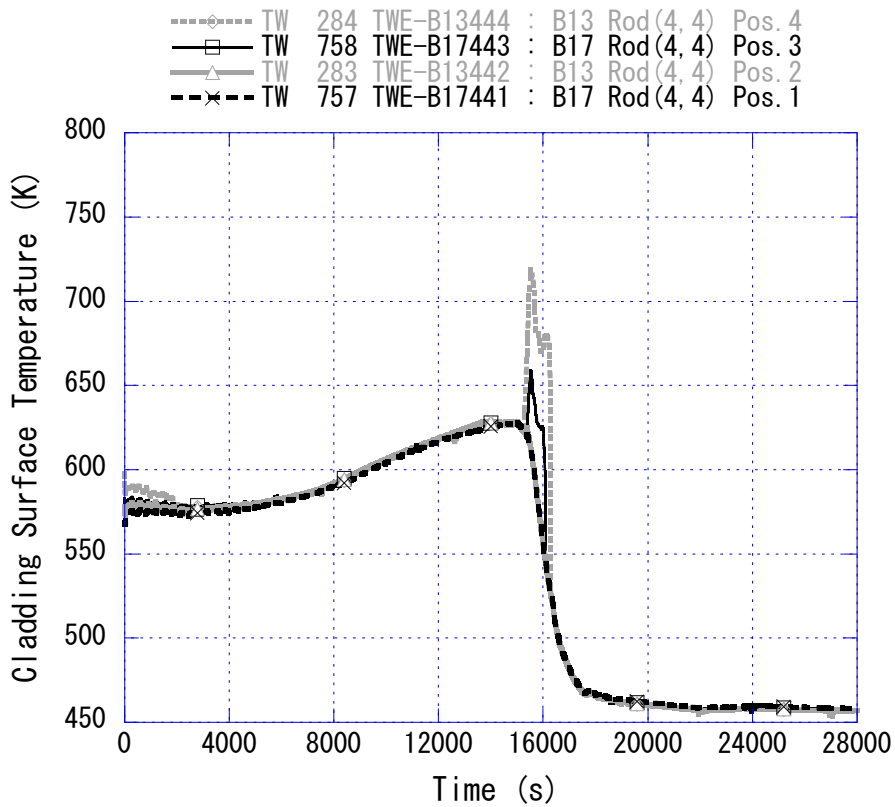


Fig. 4-26 Typical cladding surface temperatures at Positions 4-1 (0 to 28000 s)

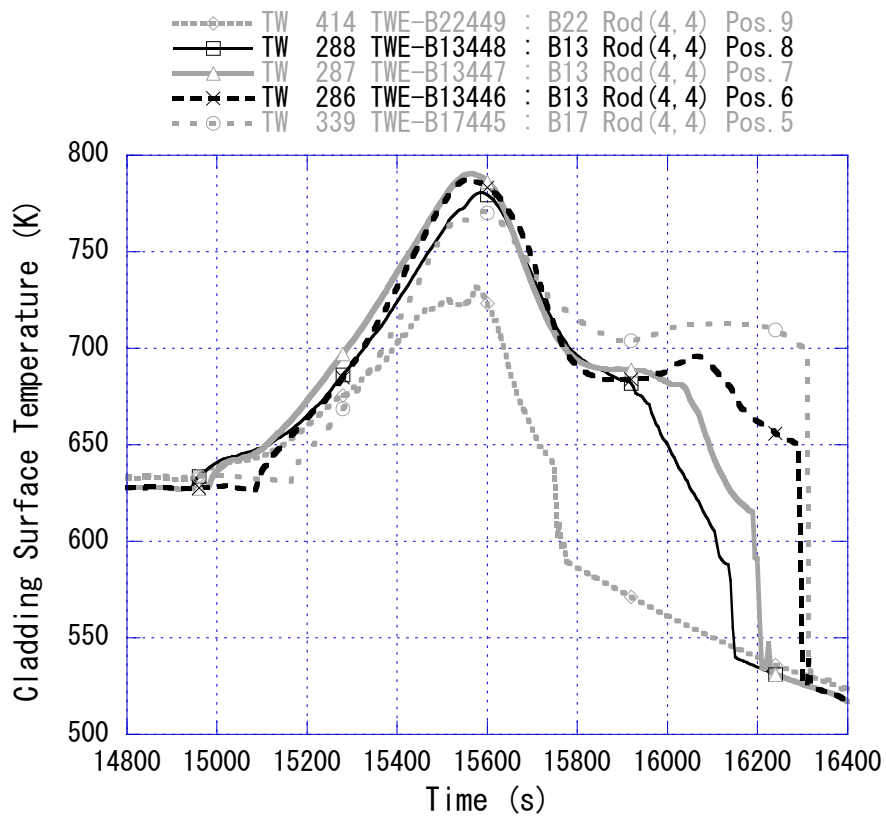


Fig. 4-27 Typical cladding surface temperatures at Positions 9-5 (14800 to 16400 s)

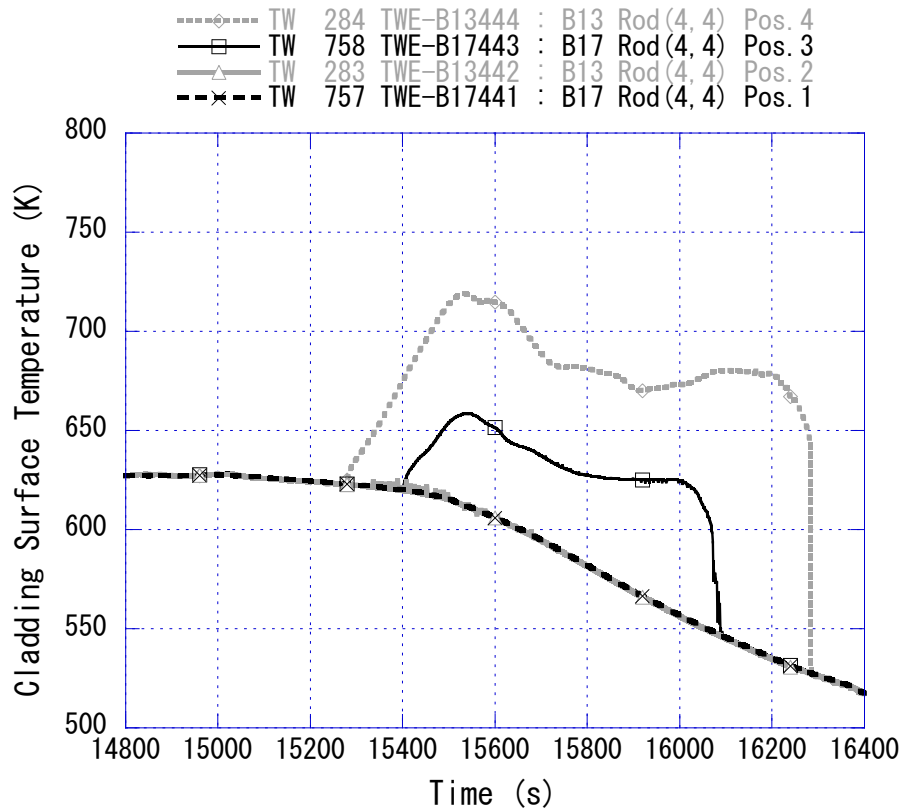


Fig. 4-28 Typical cladding surface temperatures at Positions 4-1 (14800 to 16400 s)

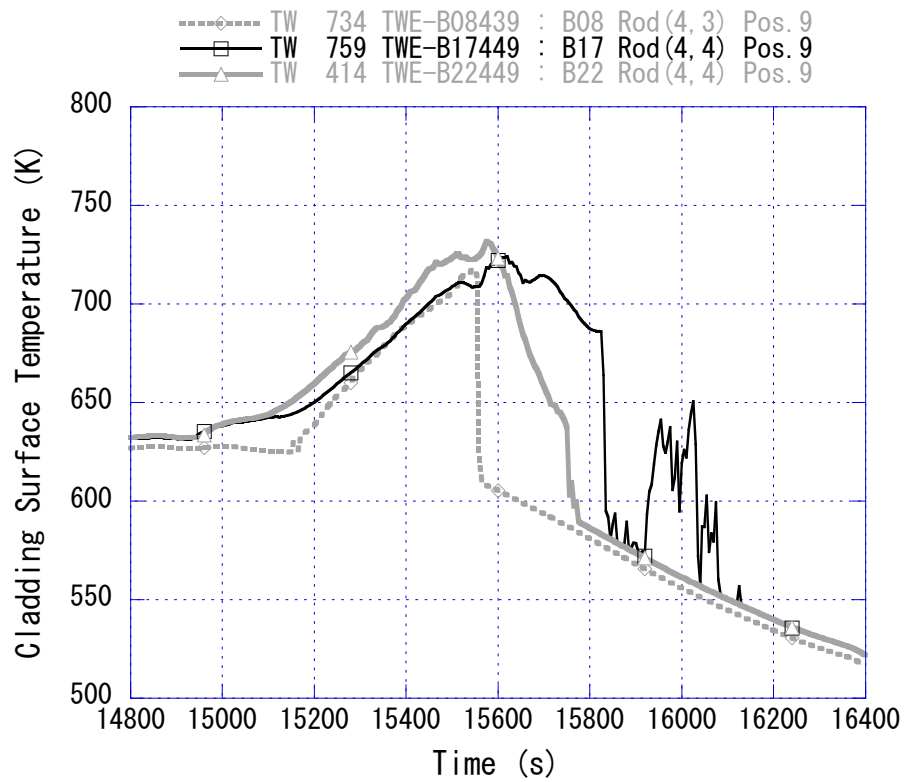


Fig. 4-29 Cladding surface temperatures at Position 9 (14800 to 16400 s)

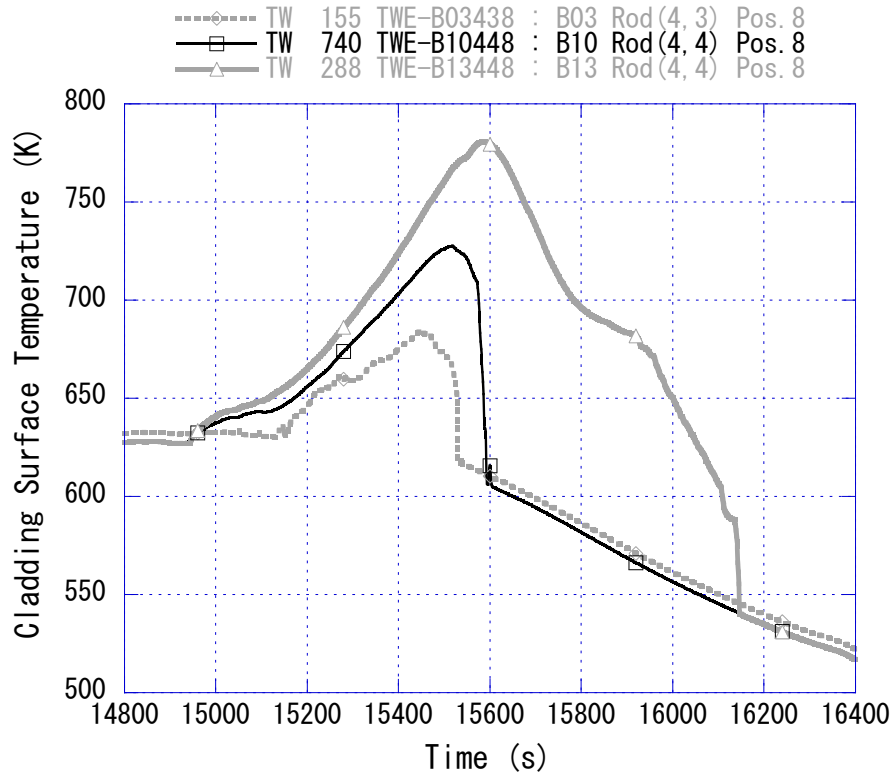


Fig. 4-30 Cladding surface temperatures at Position 8 (14800 to 16400 s)

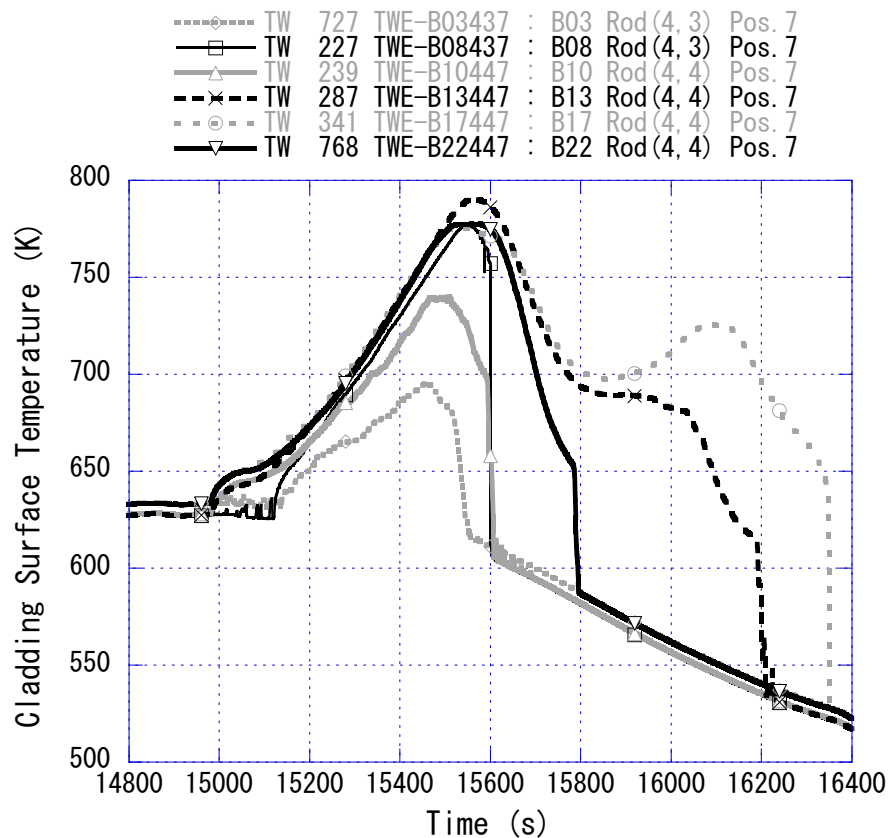


Fig. 4-31 Cladding surface temperatures at Position 7 (14800 to 16400 s)

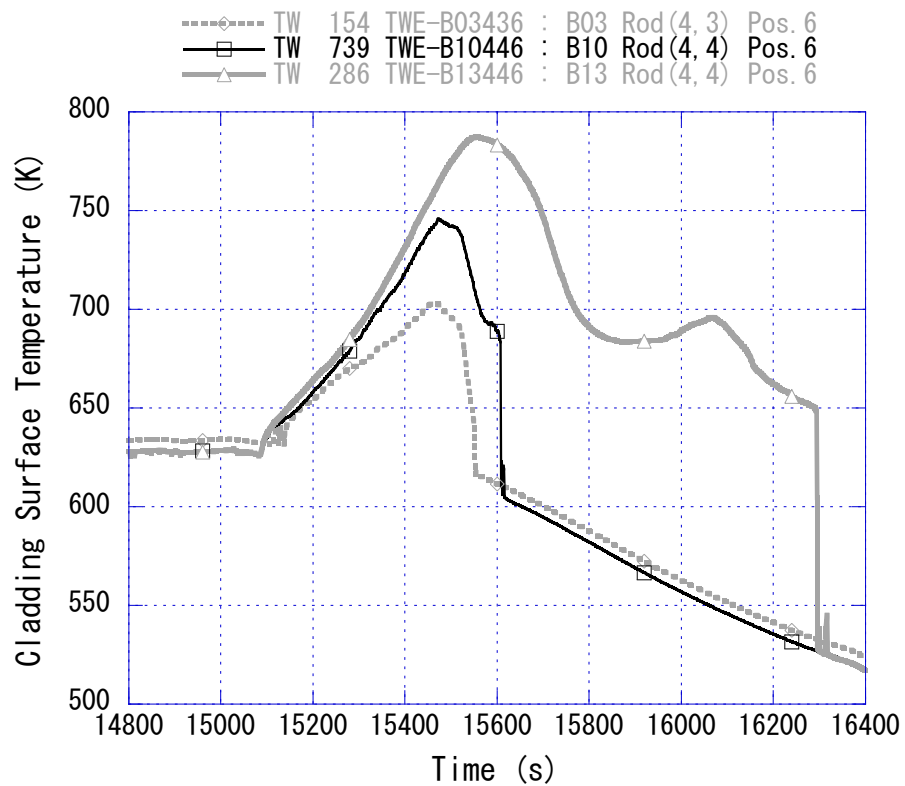


Fig. 4-32 Cladding surface temperatures at Position 6 (14800 to 16400 s)

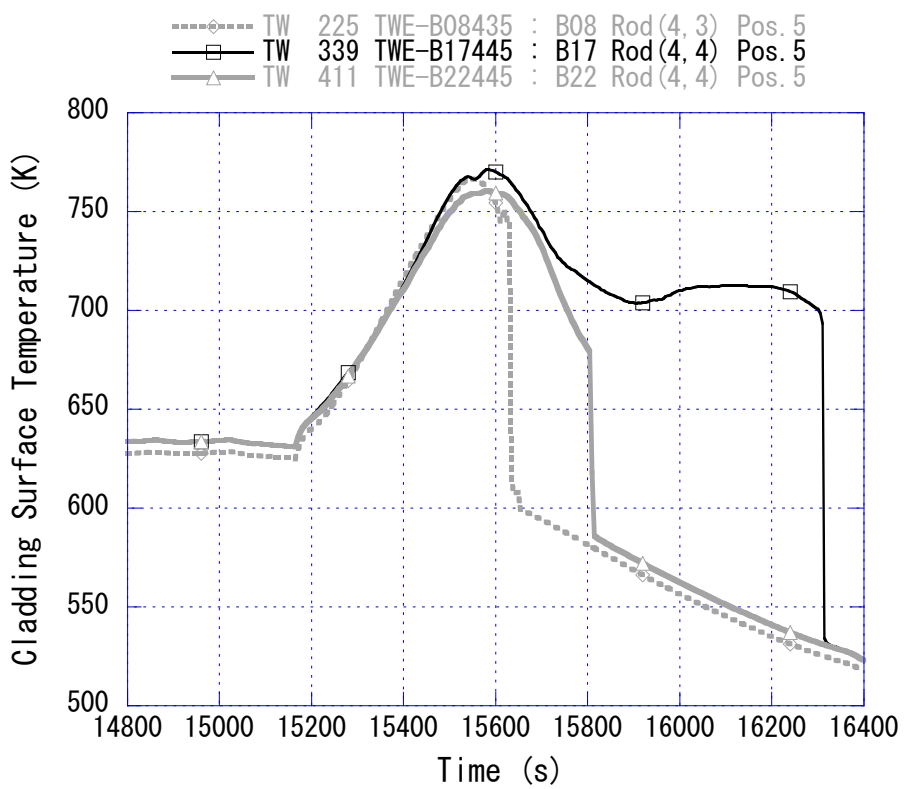


Fig. 4-33 Cladding surface temperatures at Position 5 (14800 to 16400 s)

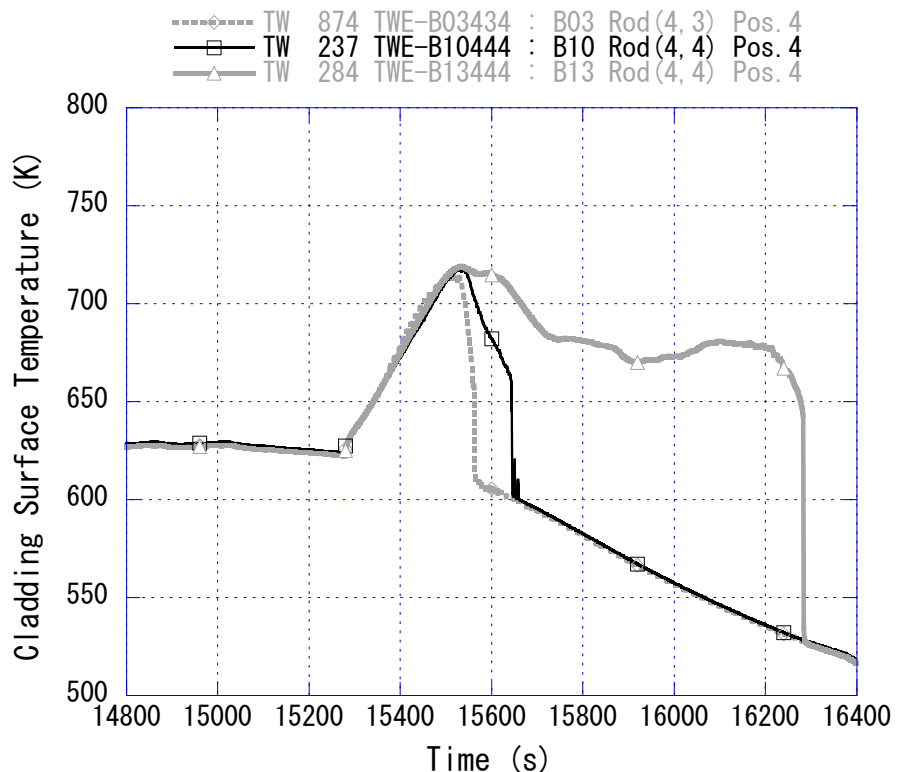


Fig. 4-34 Cladding surface temperatures at Position 4 (14800 to 16400 s)

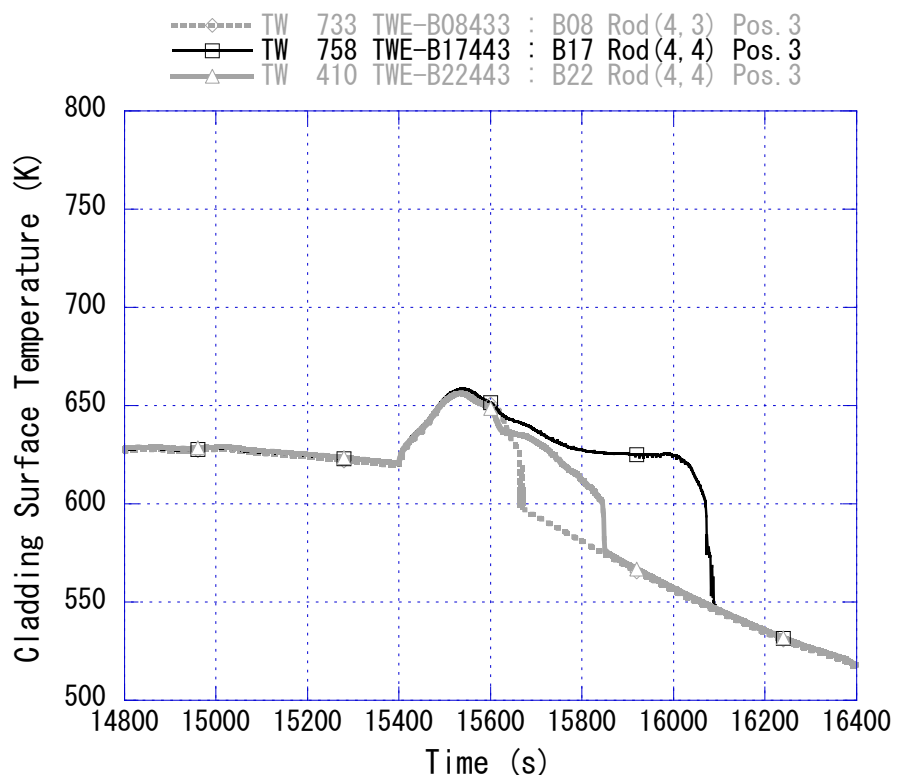


Fig. 4-35 Cladding surface temperatures at Position 3 (14800 to 16400 s)

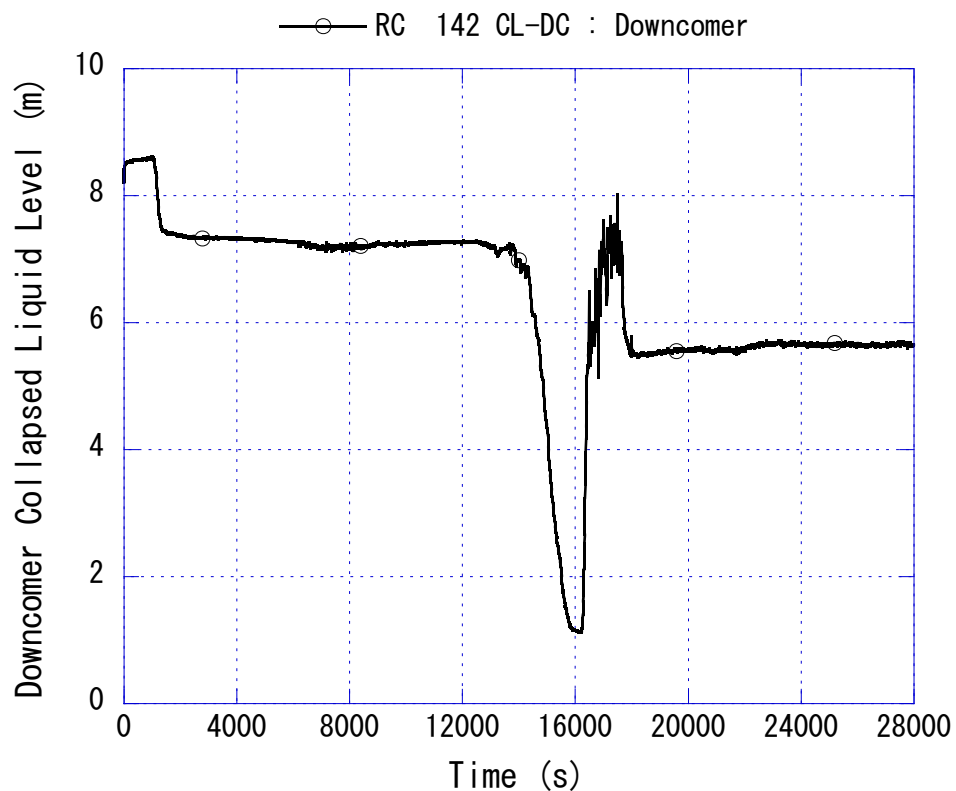


Fig. 4-36 Downcomer collapsed liquid level

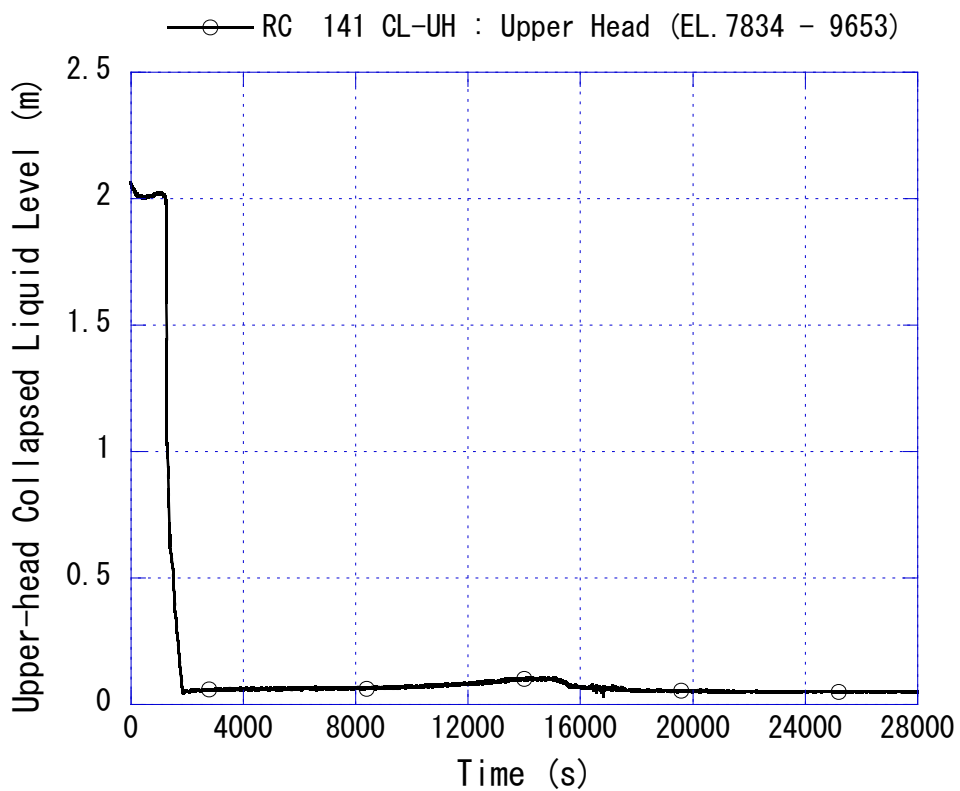


Fig. 4-37 Upper-head collapsed liquid level

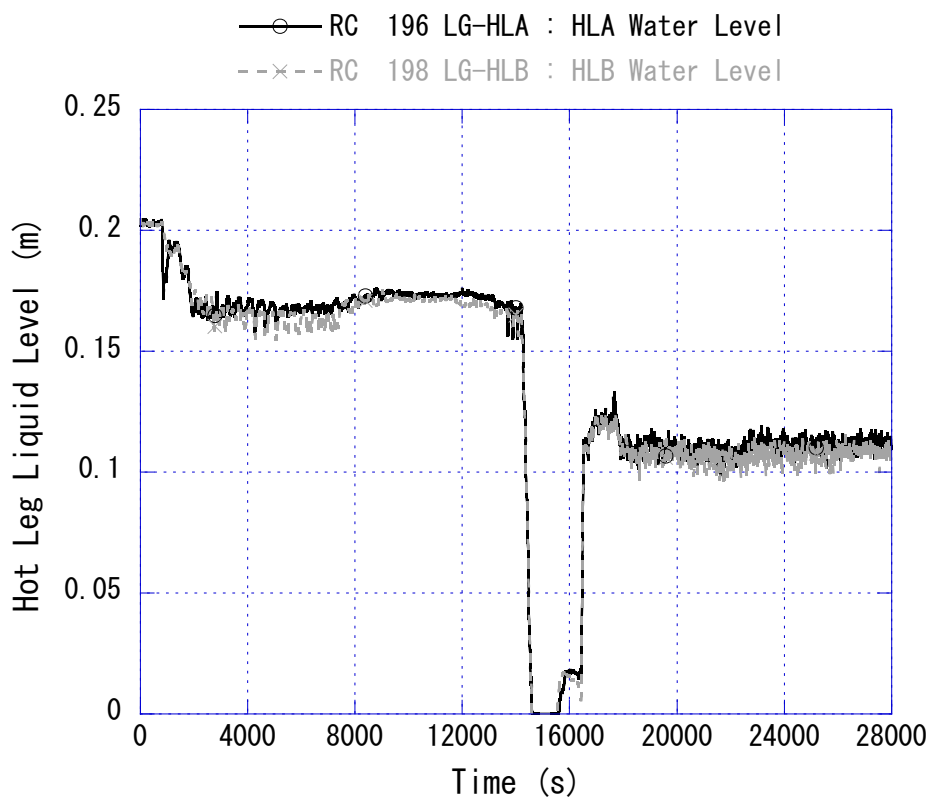


Fig. 4-38 Hot leg liquid level

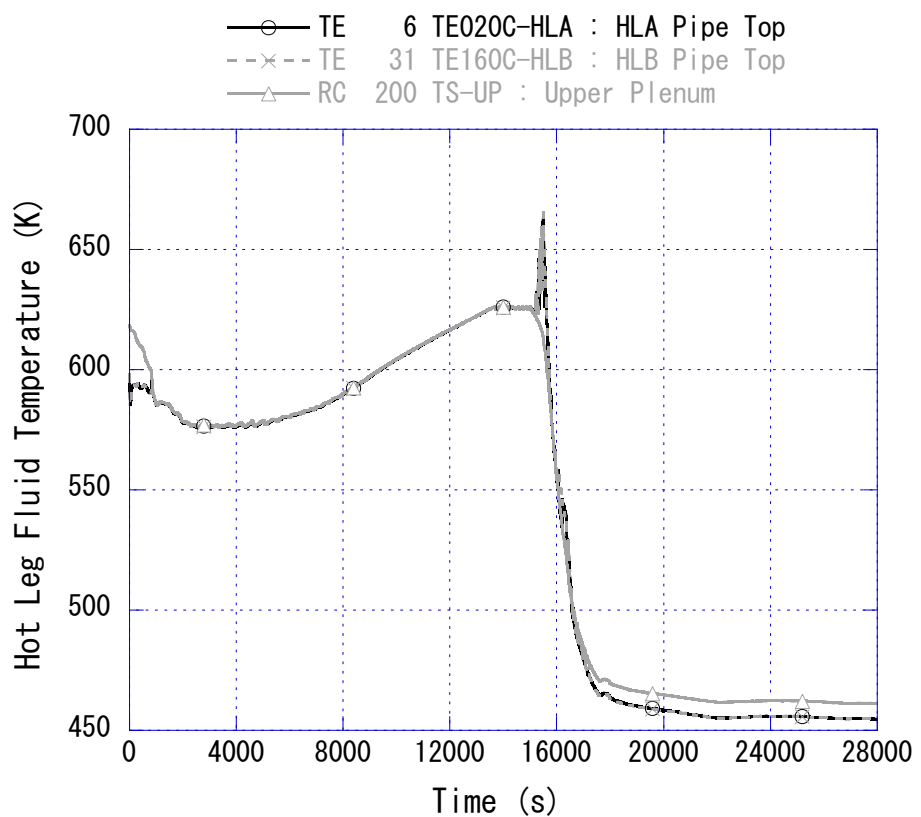


Fig. 4-39 Hot leg fluid temperature

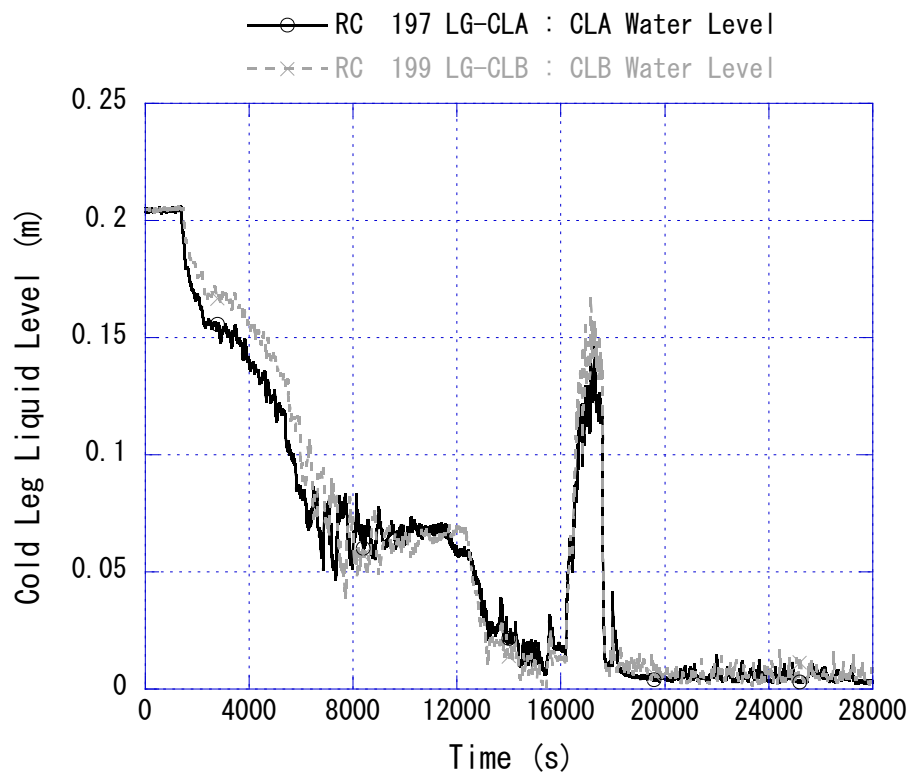


Fig. 4-40 Cold leg liquid level

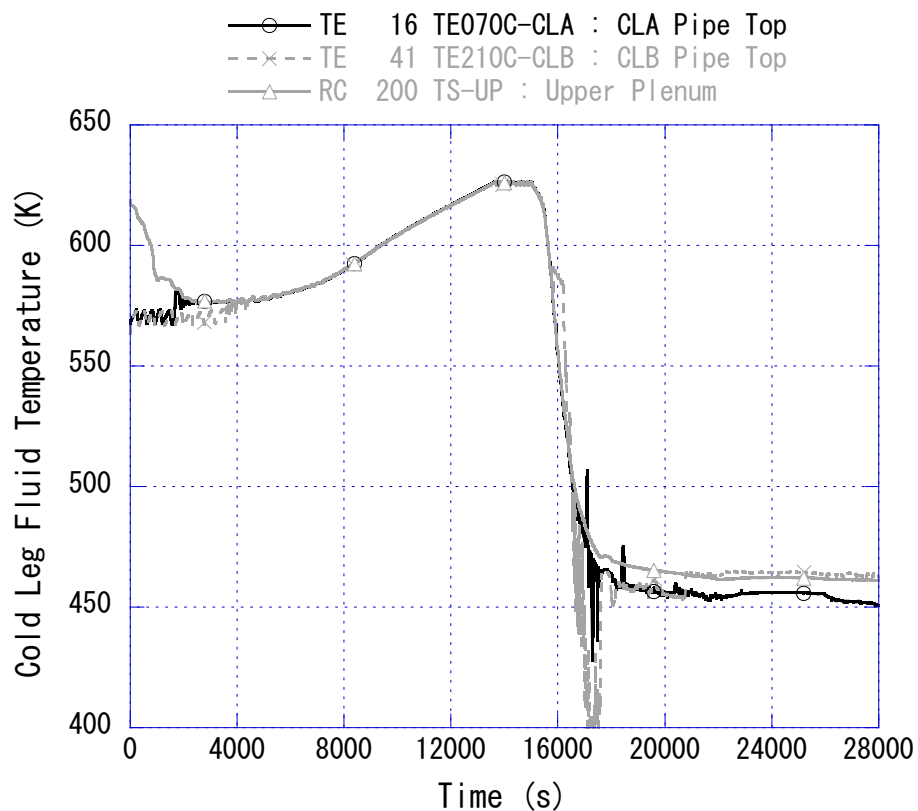


Fig. 4-41 Cold leg fluid temperature

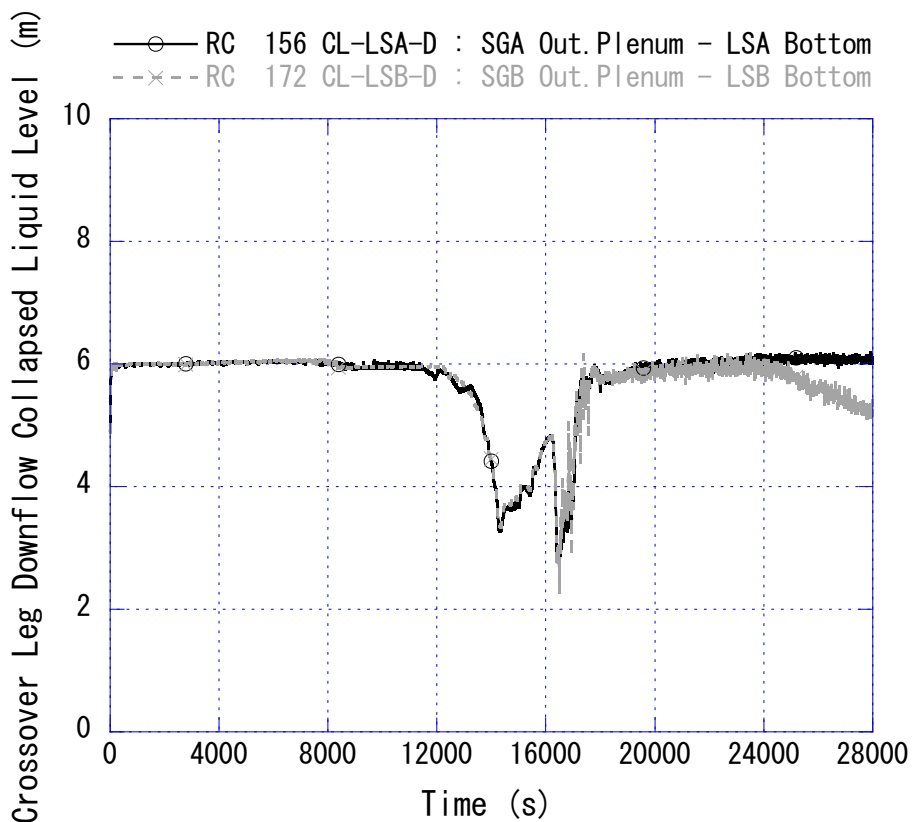


Fig. 4-42 Crossover leg downflow-side collapsed liquid level

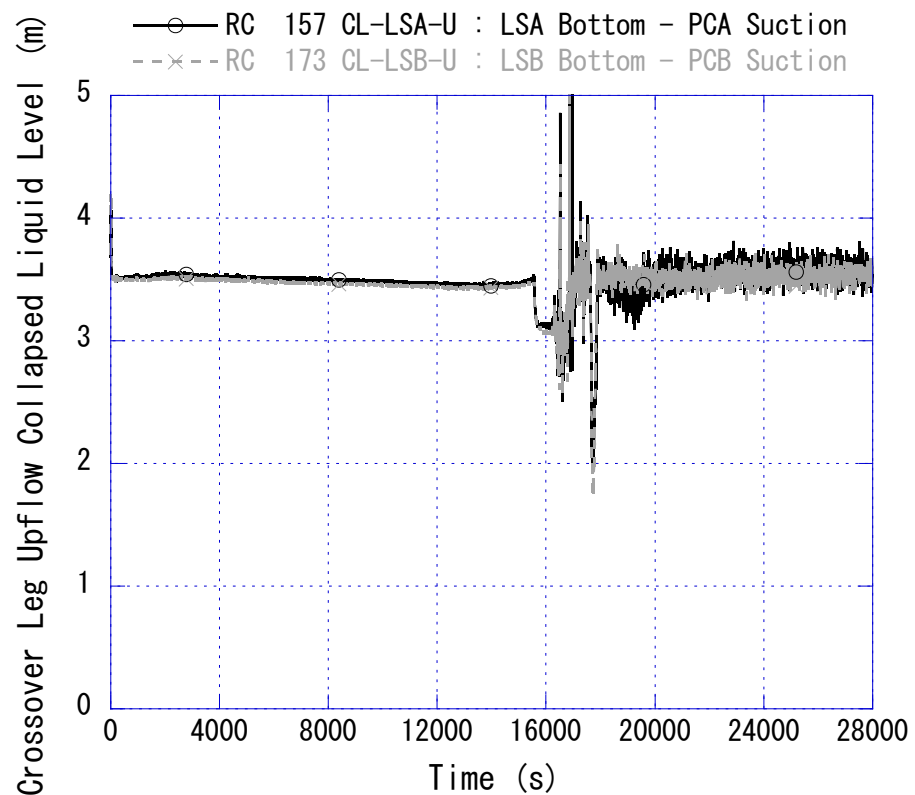


Fig. 4-43 Crossover leg upflow-side collapsed liquid level

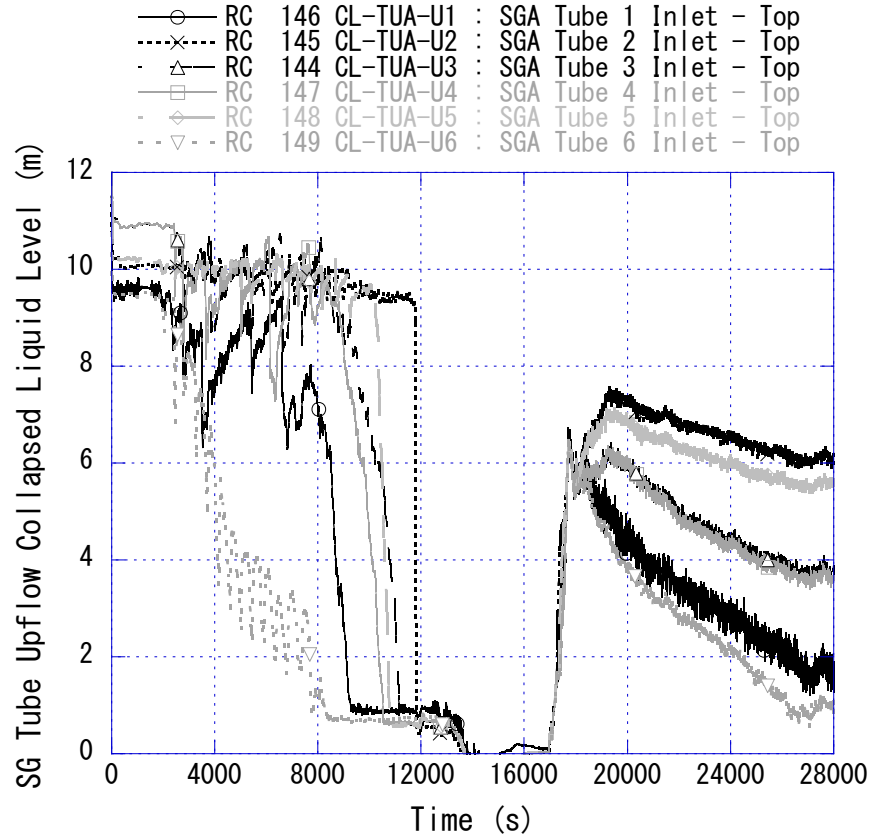


Fig. 4-44 SG U-tube upflow-side collapsed liquid level in loop with pressurizer

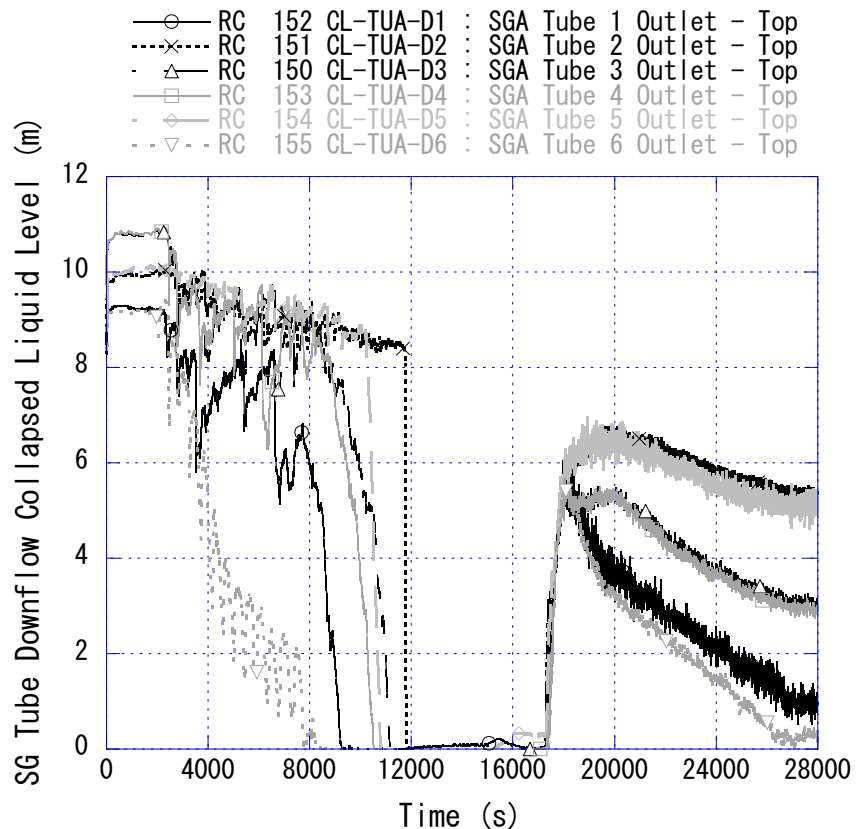


Fig. 4-45 SG U-tube downflow-side collapsed liquid level in loop with pressurizer

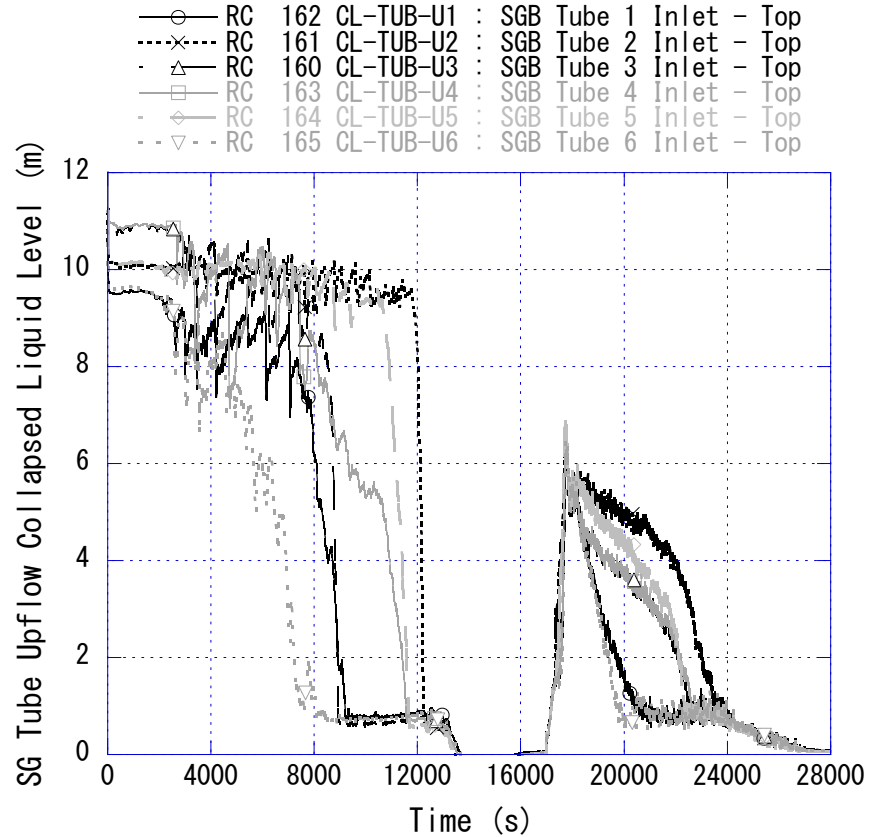


Fig. 4-46 SG U-tube upflow-side collapsed liquid level in loop without pressurizer

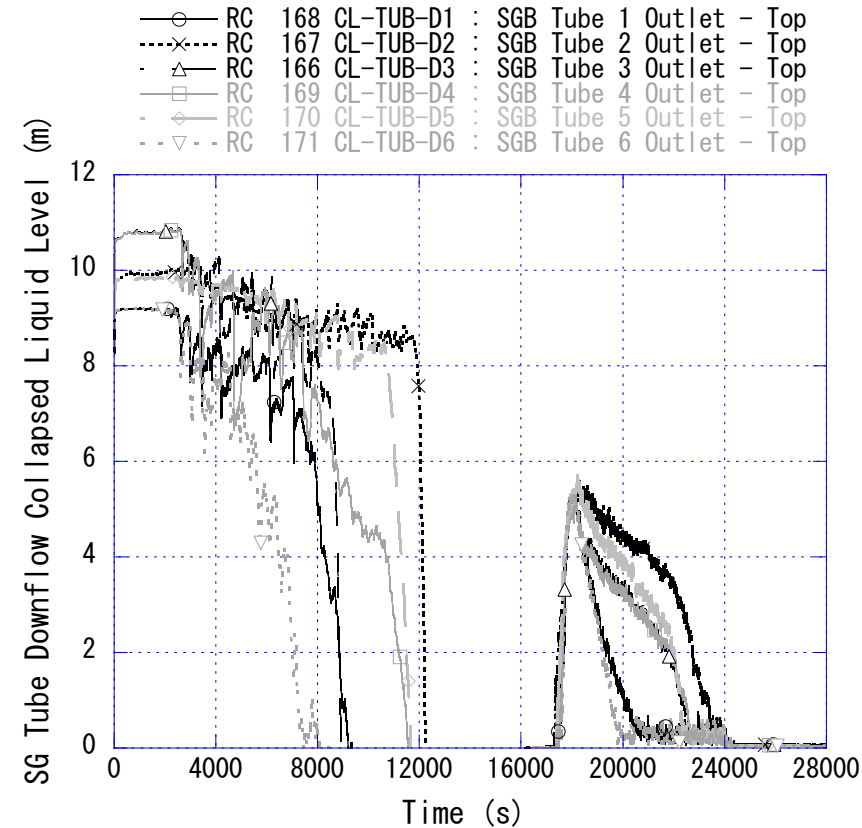


Fig. 4-47 SG U-tube downflow-side collapsed liquid level in loop without pressurizer

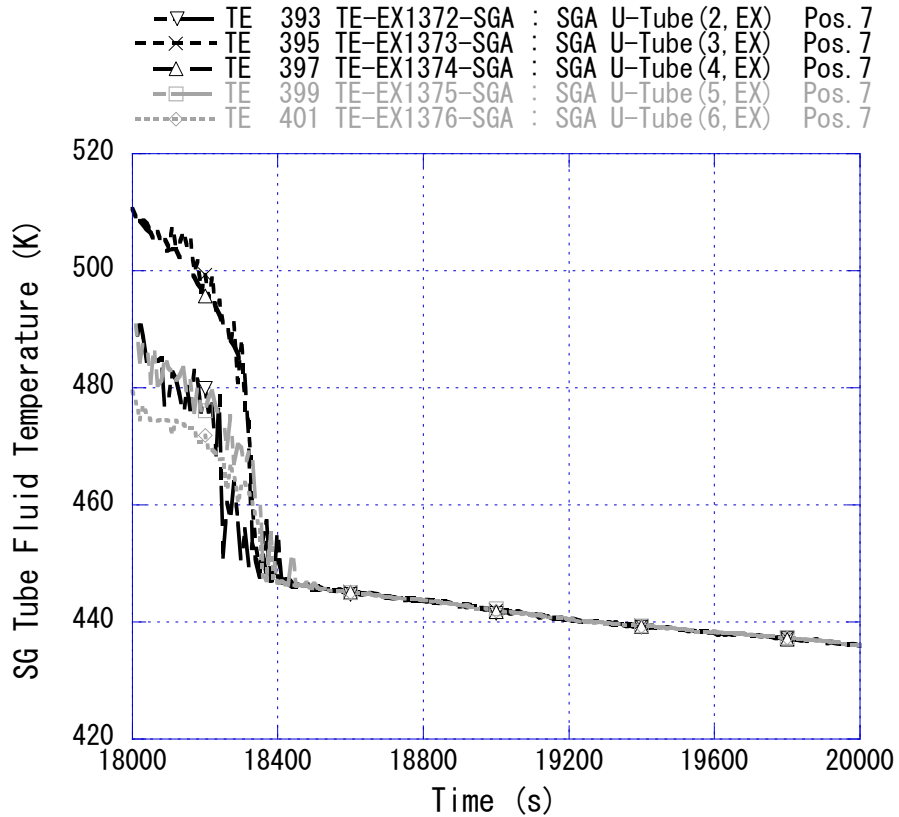


Fig. 4-48 SG U-tube downflow-side fluid temperature in loop with pressurizer

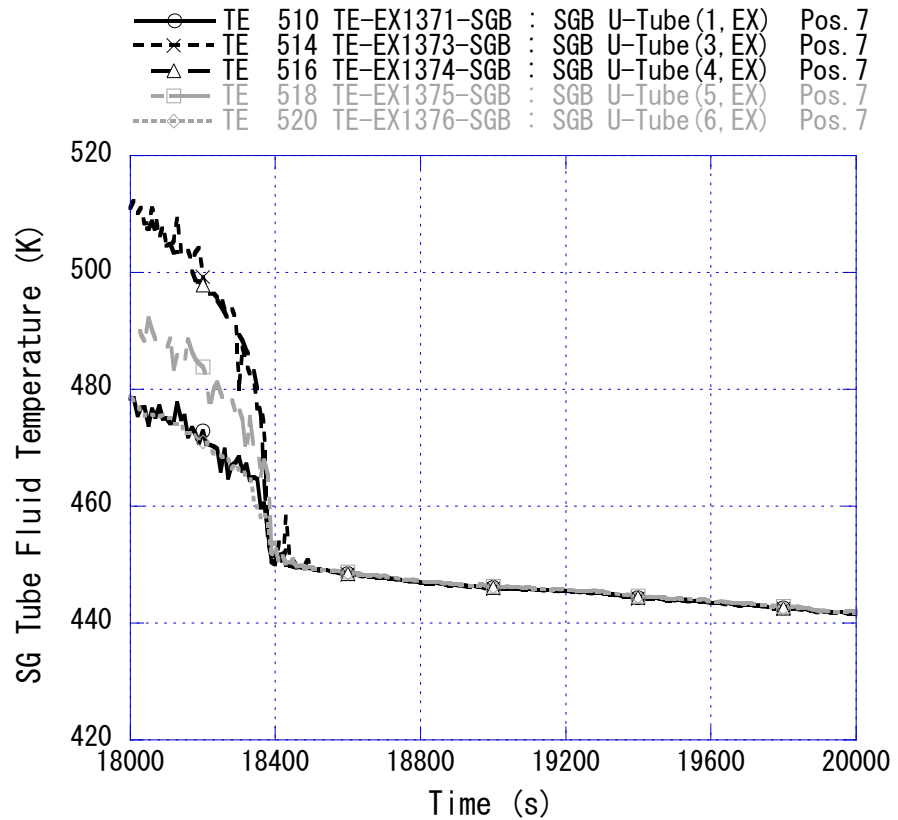


Fig. 4-49 SG U-tube downflow-side fluid temperature in loop without pressurizer

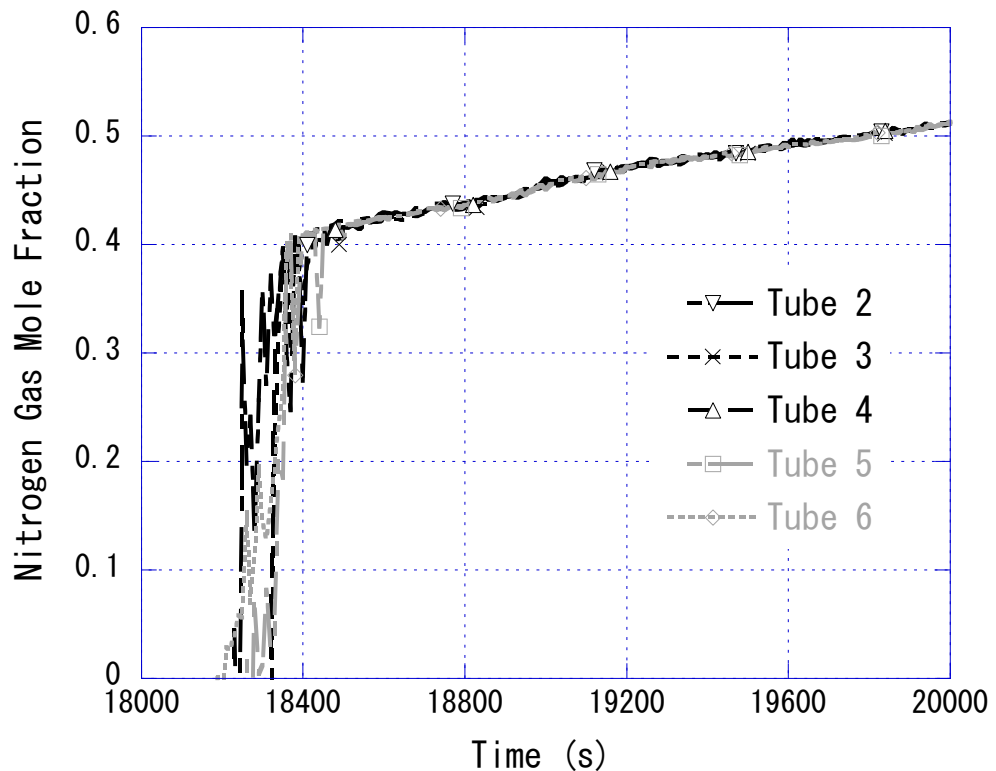


Fig. 4-50 Nitrogen gas mole fraction of SG U-tube in loop with pressurizer

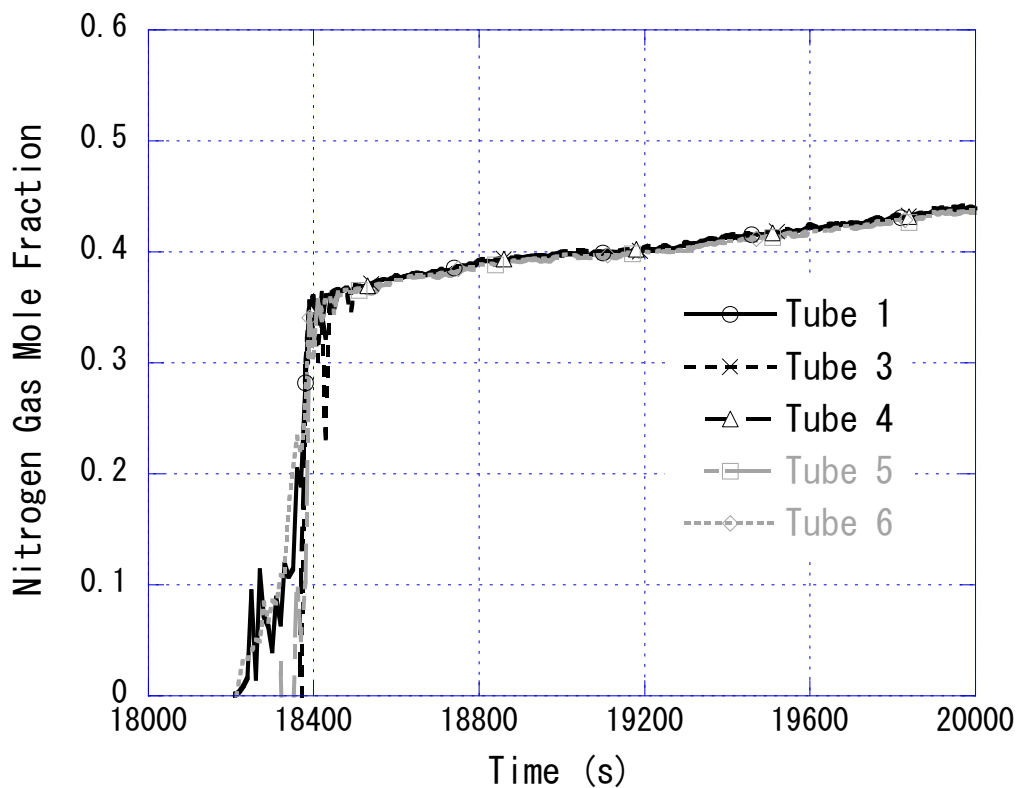


Fig. 4-51 Nitrogen gas mole fraction of SG U-tube in loop without pressurizer

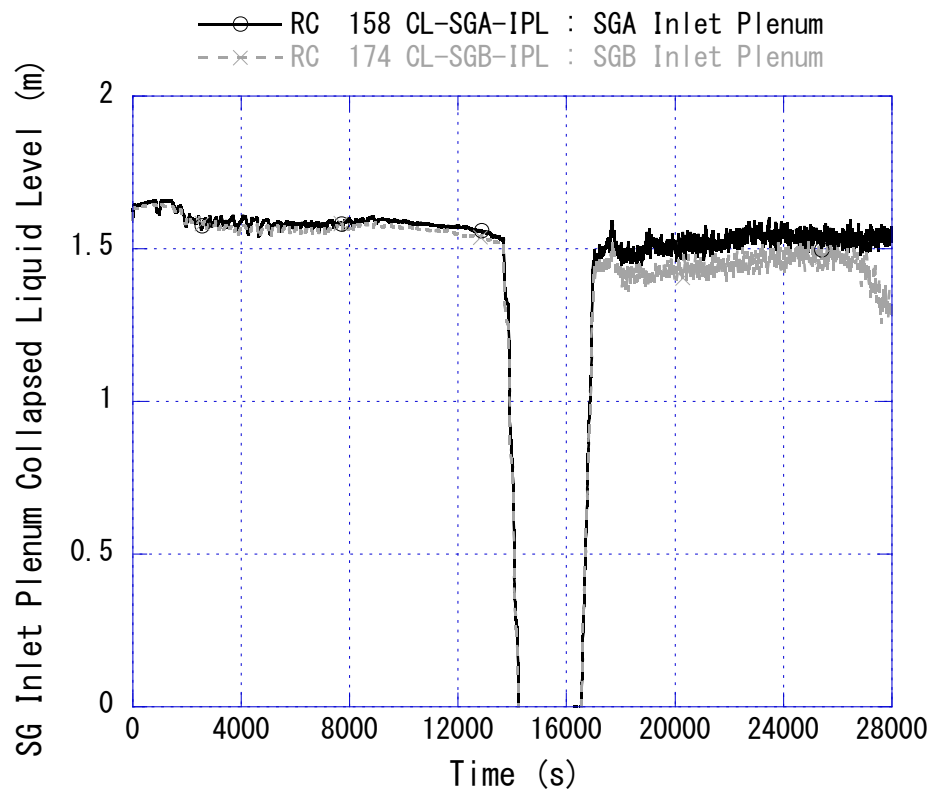


Fig. 4-52 SG inlet plenum collapsed liquid level

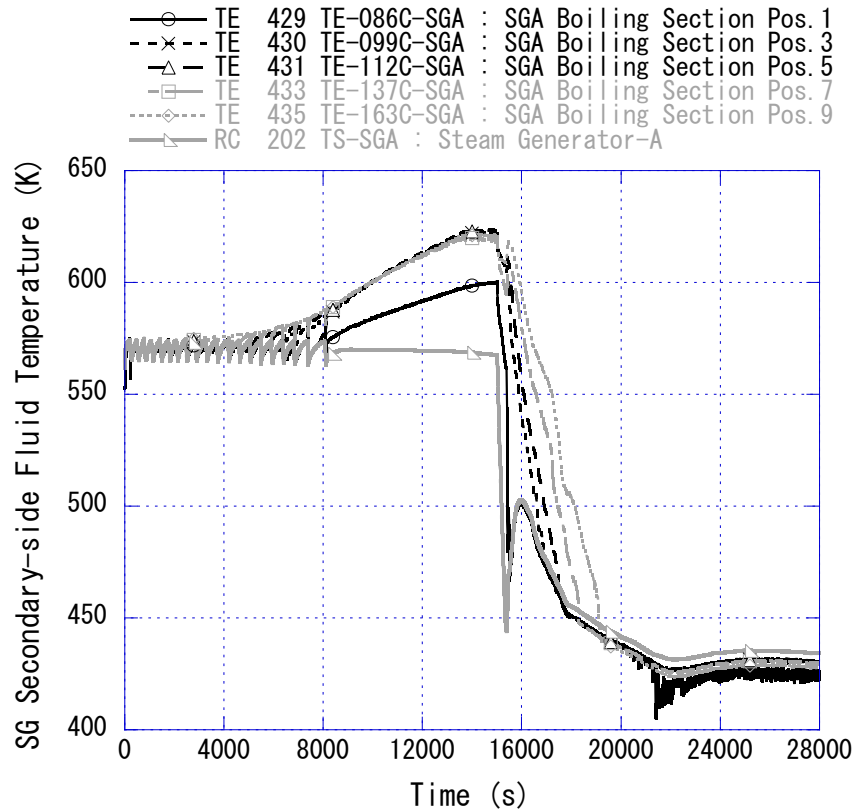


Fig. 4-53 SG secondary-side fluid temperature in loop with pressurizer

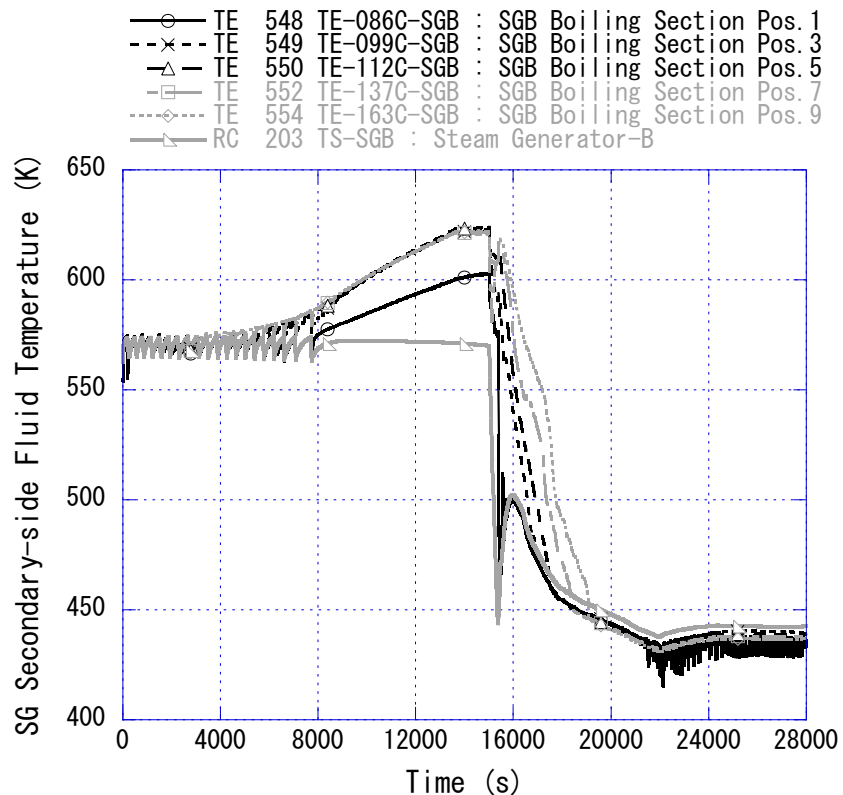


Fig. 4-54 SG secondary-side fluid temperature in loop without pressurizer

5. Summary

A ROSA/LSTF experiment named TR-LF-15 was carried out on June 11, 2014. This test simulated AM actions during a PWR SBO (TMLB' scenario) transient with pump seal LOCA. A feature of this scenario is loss of auxiliary feedwater functions. A 0.1% cold leg break was considered to simulate the pump seal LOCA. The test assumptions were made such as total failure of both high pressure injection system and low pressure injection system of ECCS. Also, non-condensable gas (nitrogen gas) ingress to the primary system from ACC tanks of ECCS was presumed. When the cladding surface temperature rise of 10 K was confirmed during core uncover, SG secondary-side depressurization was undertaken as the first AM action. This SG secondary-side depressurization was taken by fully opening the safety valves in both SGs. Primary depressurization was started by completely opening the safety valve of PZR as the second AM action with some delay after the first AM action initiation. When the SG secondary-side pressure decreased to 1.0 MPa through the first AM action, water was injected into the secondary-side of both SGs via feedwater lines utilizing low-head pumps as the third AM action. Major consequences are summarized as follows;

- (1) The primary pressure once became close to the SG secondary-side pressure following the break. When the SG secondary-side collapsed liquid level lowered to a certain low liquid level, the primary pressure turned to increase. This was owing to degradation in the heat removal from the SG secondary-side system.
- (2) The SG secondary-side liquid level became lost, and then the PZR safety valve periodically opened which induced loss of primary coolant. Core uncover thus occurred by core boil-off at high pressure. The SG secondary-side and primary pressures significantly reduced just after the first and second AM actions, respectively.
- (3) The PZR liquid level once lost, and then recovered along with the primary pressure rise. An abrupt decline began in the PZR liquid level through the primary depressurization, and thus the PZR became voided again.
- (4) A drop in the primary pressure was accelerated soon after the third AM action onset. This was due to the heat removal resumption from the SG secondary-side system arisen from the liquid level recovery in the SG secondary-side. The core was entirely quenched owing to the liquid level recovery in the core following coolant injection from the ACC system into both cold legs.
- (5) The primary depressurization rate declined due to the nitrogen gas accumulation in the SG U-tubes after the termination of the ACC system. Non-uniform flow behaviors were observed in the SG U-tubes with nitrogen gas influx.
- (6) The experiment was ended when confirming that the primary depressurization worsened on account of deterioration in the condensation heat transfer in the SG U-tubes.

Acknowledgement

The author would like to thank Messrs. I. Ohtsu and A. Ohwada of Japan Atomic Energy Agency for performing the LSTF TR-LF-15 test under collaboration with members from Nuclear Engineering Co., Ltd. as well as Miss K. Toyoda of Frontier System Co., Ltd. for manipulating the experimental data. The author is grateful to Dr. Y. Park of Korea Atomic Energy Research Institute for her useful comments to improve the manuscript.

References

- [1] Kukita, Y., Anoda, Y., Tasaka, K., Summary of ROSA-IV LSTF first-phase test program – Integral simulation of PWR small-break LOCAs and transients –, Nuclear Engineering and Design, 131(1), 1991, pp. 101-111.
- [2] Takeda, T., Nakamura, H., RELAP5 code study of ROSA/LSTF experiment on a PWR station blackout (TMLB') transient, Mechanical Engineering Journal, 1(4), Paper No. 13-00324, 2014, 13p.
- [3] Takeda, T., Ohtsu, I., ROSA/LSTF experiment on a PWR station blackout transient with accident management measures and RELAP5 analyses, Mechanical Engineering Journal, 2(5), Paper No. 15-00132, 2015, 15p.
- [4] USNRC, Reactor safety study – An assessment of risks in U.S. commercial nuclear power plants, WASH-1400, NUREG-075/14, 1975.
- [5] The ROSA-V Group, ROSA-V Large Scale Test Facility (LSTF) System Description for the Third and Fourth Simulated Fuel Assemblies, JAERI-Tech 2003-037, 2003, 479p.
- [6] NRA, Analyses of Events for the Evaluation of the Effectiveness of Measures against Severe Core Damage (PWR), NTEC-2014-1001, 2014, 141p. (in Japanese).
- [7] Svendsen, S., Passive thermal shutdown seal enhances safety of nuclear plants, Sealing Technology, 2012(3), 2012, 2p.
- [8] Mena-Rosell, L., Queral, C., Ruiz-Zapatero, M., et al., Analysis of PWR SBO sequences with RCP passive thermal shutdown seals, Journal of Nuclear Science and Technology, 55(6), 2018, pp. 649-662.
- [9] Hsu, H.T., Chen, C.H., Lo, C.K., Risk reduction assessment for installing RCP shutdown seal, Nuclear Technology, 206(12), 2020, pp. 1891-1908.

- [10] Watanabe, T., Kukita, Y., Experiment and analyses of PWR station blackout transient involving pump seal leak, Proceedings of the 6th International Topical Meeting on Nuclear Reactor Thermal Hydraulics (NURETH-6), Grenoble, France, 1993, pp. 1232-1239.
- [11] Choi, K.Y., Kang, K.H., Song, C.H., Recent achievement and future prospects of the ATLAS program, Nuclear Engineering and Design, 354, Article ID 110168, 2019, 10p.
- [12] Takeda, T., Data Report of ROSA/LSTF Experiment SB-PV-07 – 1% Pressure Vessel Top Break LOCA with Accident Management Actions and Gas Inflow –, JAEA-Data/Code 2018-003, 2018, 60p.
- [13] Zuber, N., Problems in modeling small break LOCA, Technical Report, NUREG-0724, 1980.
- [14] Kumamaru, H., Tasaka, K., Recalculation of simulated post-scram core power decay curve for use in ROSA-IV/LSTF experiments on PWR small-break LOCAs and transients, JAERI-M 90-142, 1990, 63p.

Appendix A Available Experimental Data List

Table A-1 shows the list of available experimental data qualified as “Good” for LSTF TR-LF-15 (Run ID designated to be LFF). This table contains Sequential No., Function ID., Tag Name, measurement location, range, unit, and uncertainty. The alphabetical prefix of the Function ID. and Tag Name is explained as follows;

- (1) TE, fluid temperature,
- (2) DT, differential temperature,
- (3) TW, heater rod and structure temperature,
- (4) FE, flow rate measured with conventional (differential pressure) flow meters,
- (5) PE, pressure,
- (6) MI, miscellaneous instrumented-signal (power, pump rotation speed, etc.),
- (7) LE, liquid level,
- (8) DP, differential pressure,
- (9) DE, fluid density measured with gamma-ray densitometer,
- (10) RC, two-phase flow data calculated with DE and others.

Table A-1 (Cont'd)

SEQ No.	Function ID.	Tagname	Location	Range		Unit	Uncertainty	
				LO	HI		± ABS.	± %FR
1549	RC 157	CL-LSA-U	LSA Bottom - PCA Suction	-	-	m	0.188	-
1550	RC 158	CL-SGA-IPL	SGA Inlet Plenum	-	-	m	0.185	-
1551	RC 159	CL-HLB-SGB	HLB Riser Part	-	-	m	0.179	-
1552	RC 160	CL-TUB-U3	SGB Tube 3 Inlet - Top	-	-	m	0.445	-
1553	RC 161	CL-TUB-U2	SGB Tube 2 Inlet - Top	-	-	m	0.433	-
1554	RC 162	CL-TUB-U1	SGB Tube 1 Inlet - Top	-	-	m	0.73	-
1555	RC 163	CL-TUB-U4	SGB Tube 4 Inlet - Top	-	-	m	0.74	-
1556	RC 164	CL-TUB-U5	SGB Tube 5 Inlet - Top	-	-	m	0.734	-
1557	RC 165	CL-TUB-U6	SGB Tube 6 Inlet - Top	-	-	m	0.73	-
1558	RC 166	CL-TUB-D3	SGB Tube 3 Outlet - Top	-	-	m	0.951	-
1559	RC 167	CL-TUB-D2	SGB Tube 2 Outlet - Top	-	-	m	0.74	-
1560	RC 168	CL-TUB-D1	SGB Tube 1 Outlet - Top	-	-	m	0.735	-
1561	RC 169	CL-TUB-D4	SGB Tube 4 Outlet - Top	-	-	m	0.747	-
1562	RC 170	CL-TUB-D5	SGB Tube 5 Outlet - Top	-	-	m	0.74	-
1563	RC 171	CL-TUB-D6	SGB Tube 6 Outlet - Top	-	-	m	0.735	-
1564	RC 172	CL-LSB-D	SGB Out.Plenum - LSB Bottom	-	-	m	0.207	-
1565	RC 173	CL-LSB-U	LSB Bottom - PCB Suction	-	-	m	0.188	-
1566	RC 174	CL-SGB-IPL	SGB Inlet Plenum	-	-	m	0.094	-
1567	RC 175	MC-UH	Upper Head (EL.6614 - 9653)	-	-	kg	79.08	-
1568	RC 176	MC-LSA-DW	SGA Out.Plenum+LSA Downflow	-	-	kg	42.68	-
1569	RC 177	MC-LSB-DW	SGB Out.Plenum+LSB Downflow	-	-	kg	41.33	-
1570	RC 178	MS-CORE	Core (EL.-35 - 3945)	-	-	kg	15.4	-
1571	RC 179	MS-UP	Upper Plenum (EL.4060 - 6135)	-	-	kg	24.37	-
1572	RC 180	MS-DC	Downcomer	-	-	kg	46.31	-
1573	RC 181	MS-TUA-UP-AV	SGA Tubes Upflow side	-	-	kg	8.3	-
1574	RC 182	MS-TUA-DW-AV	SGA Tubes Downflow side	-	-	kg	8.3	-
1575	RC 183	MS-SGA-IPL	SGA Inlet Plenum	-	-	kg	27.81	-
1576	RC 184	MS-LSA-UP	LSA Upflow side	-	-	kg	3.57	-
1577	RC 185	MS-TUB-UP-AV	SGB Tubes Upflow side	-	-	kg	9.65	-
1578	RC 186	MS-TUB-DW-AV	SGB Tubes Downflow side	-	-	kg	10.25	-
1579	RC 187	MS-SGB-IPL	SGB Inlet Plenum	-	-	kg	14.61	-
1580	RC 188	MS-LSB-UP	LSB Upflow side	-	-	kg	3.57	-
1581	RC 189	MS-ACC	Acc-Cold Tank	-	-	kg	39.26	-
1582	RC 190	MS-ACH	Acc-Hot Tank	-	-	kg	74.26	-
1583	RC 191	MS-ST	Break Flow Supp. Tank	-	-	kg	323.61	-
1584	RC 192	DM-ACC	Acc-Cold Tank	-	-	kg/s	13.55	-
1585	RC 193	DM-ACH	Acc-Hot Tank	-	-	kg/s	26.08	-
1586	RC 194	IM-ST	Break Flow Supp. Tank	-	-	kg/s	3.35	-
1587	RC 195	DM-RWST	RWST	-	-	kg/s	51.9	-
1588	RC 196	LG-HLA	HLA Water Level	-	-	m	0.012	-
1589	RC 197	LG-CLA	CLA Water Level	-	-	m	0.028	-
1590	RC 198	LG-HLB	HLB Water Level	-	-	m	0.012	-
1591	RC 199	LG-CLB	CLB Water Level	-	-	m	0.028	-
1592	RC 200	TS-UP	Upper Plenum	-	-	K	17.64	-
1593	RC 202	TS-SGA	Steam Generator-A	-	-	K	7.82	-
1594	RC 203	TS-SGB	Steam Generator-B	-	-	K	7.82	-
1595	RC 236	IM-IRWST	IRWST	-	-	kg/s	-	-
1596	RC 279	DE291-SGB-EU	SGB Feedwater Line	-	-	kg/m³	-	-
1597	RC 296	IM-IRWSTL	IRWST	-	-	kg/s	-	-

This is a blank page.

